Author comments (AC) and manuscript changes (MC) on interactive comment by K. Mahan

(kevin.mahan@colorado.edu)

1) *The first has to do with organization and lack of necessary background information. Much of the necessary information appears to have been published already in Wex et al. (2017, Tectonics), but more than citations to that work need to be presented here. For example, there is a distinct need for some description of the "starting material" that was reworked in this shear zone, or at least some description of representative lithologies, assemblages, and estimated equilibrium conditions for those starting assemblages (presumably Musgravian). This has important implication for the authors' interpretation that the fluid source was the lower plate and that the shear zone system was essentially "closed." The lower plate rock is currently described as "upper amphibolite-facies during Musgravian without further details. But were these rocks reworked by the Woodroffe deformation in a retrograde or prograde sense? If prograde, then they could conceivably produce free fluid internally through dehydration reactions. But if in a retrograde sense, then they would have consumed water, if present, rather than produce it.*

AC/MC: Our geological introduction was indeed very concise. Following the reviewer's suggestion, we have extended the geological introduction of the manuscript to provide additional information regarding the Musgravian Orogeny "starting material" and the estimated metamorphic conditions, also in comparison to the metamorphic overprint during the Petermann Orogeny.

---

2) *The authors could call upon dehydration-driven fluids from deeper levels in the footwall, but then it is not a "closed system." The whole calcite and O and C isotope story seems to point to an external source of fluid too.*

AC: Carbon indeed cannot have an immediately local source, because the studied rocks are initially entirely non-carbonaceous. With regard to carbon the system is clearly not closed. We tried to further constrain the origin using stable isotopes. Unfortunately, the whole calcite isotope story is not conclusive, and our current conclusions based on this data therefore rather speculative. However, our observations and data clearly indicate that the source of the hydrous fluids and that of carbon are not the same. The external carbon source does therefore not provide any constraints for the source of the hydrous fluids. We do not argue that dehydration-driven fluids originate from deep levels in the footwall, but immediately from within the local, exposed footwall units. This would represent a closed system with regard to the aqueous fluids.

MC: The interpretation of the calcite isotopic data, has been formulated into more restrained statements (see comment 25) and moved to the appendix in the revised version.

---

3) *Some clarification is needed, and probably a summarization of what Wex et al. (2017) learned about these rocks in the previous study would help a lot.*

AC: Where necessary, Wex et al. (2017) is cited and, where appropriate, we now provide additional information, e.g. that P-T conditions were determined via conventional geothermobarometry rather than just stating the derived numbers. We have avoided providing an extensive and detailed report of the results previously published in Wex et al. (2017), as that would result in unnecessary lengthening of the manuscript. The current manuscript was submitted subsequently to the published companion paper of Wex et al. (2017) in order to allow a systematic development and avoid repetition of previously published data.

MC: Additional information on how Wex et al. (2017) constrained the syn-kinematic P-T conditions and the interpreted meaning of these values has been added.

---

4) *This suggestion extends to the pseudotachylyte system as well, which is used in the current study but with very little description what their role in the evolution of the shearing history is.*

AC: The pseudotachylyte system and associated microstructures are only of marginal relevance to the current paper, which is why they were not presented in full detail. These aspects will be thoroughly presented in a follow-up companion paper, which particularly focuses on the brittle-ductile interplay (pseudotachylytes vs. mylonites) and pseudotachylyte development at mid-crustal depths. The proposed manuscript has already been compiled and is ready for submission once the current manuscript is published. The current manuscript will provide some relevant background information for this forthcoming paper, as the paper by Wex et al. (2017) has provided necessary background information for the current submission.

---

5) *The authors mention evidence for two stages of deformation at different conditions in the shear zone and give P-T conditions, but does that really reflect distinctly different time periods?*

AC: The mentioned two stages of deformation are differentiated on the basis of microstructure and petrology and interpreted to represent different time periods during shearing along the Woodroffe Thrust, as discussed in detail in Wex et al (2017). We agree that mentioning this aspect might be confusing to the reader, because it is not crucial in the current manuscript.

MC: Since this information is not relevant to the current manuscript we have omitted those parts making reference to the presence of two different stages of deformation.

6) *What is the basis for "regional temperature gradient" that is shown in Fig. 8 and 10??? There is no description of where that came from other than a citation to Wex et al. (2017), but it basis is pretty critical this proposed story and interpretations here too.*

AC: As discussed in comment 3), we have now added the information that P-T conditions were constrained from conventional geothermobarometry. We provide this information where we first referenced Wex et al. (2017) in reference to the estimated P-T conditions. Then, for subsequent references to the temperature gradient and to the P-T estimates (for instance in Fig. 8 and 10), a simple reference to Wex et al. (2017) should be sufficient.

MC: Additional information on how Wex et al. (2017) constrained the syn-kinematic P-T conditions and the interpreted meaning of these values has been added.

---

7) *I suggest the authors start early in the manuscript with a description of the sampling strategy as essentially on a N-S transect like that shown at the bottom of the current Fig. 8 – that is easy to see and easy to keep referring to, but show it in a simplified form earlier than in the 8th figure.*

AC: The locations of all samples are clearly given in Figure 1, the very first figure of the paper.

MC: In section 3, we now state explicitly that samples were collected "along a N-S traverse, parallel to the direction of thrusting".

---

8) *Right now, the fact that sample localities are broken into various northern and southern plus/minus central groups based on different datasets is convoluted. For the bulk Th measurements, "northern" is locations 1 through 6. According to Fig. 8, station 7 is plots more northerly than 6 so you really should include 7 too. But for plagioclase stability, "northern" is stations 1 through 9. And for abundance of hydrous minerals, "northern" is only stations 1 through 5. Stop all of the group attempts and simply show how the various observations and data change along the transect – the trends will be the same and much easier to follow.*

AC: We agree that this is aspect can cause confusion to the reader.

MC: We followed the reviewer's suggestion and stopped our attempts of grouping locations. We now only refer to trends.

---

9) *The final major point is that the beginning of the discussion on feldspar breakdown reactions and fluid activity in sections 8.1 and 8.2 is vague and not particularly strong. How can reactions 1 and 2 be pitted against one another when they reflect different chemical systems? One has K in it and the other does not. There is another vague reference to Wex et al. (2017) for plagioclase chemical variability during recrystallization (dynamic?) but no details – this information is important to the discussion and should be explained in more detail, either here or earlier in the manuscript in a summary of the earlier study.*

AC: We only pit reactions 3 and 4 against each other as these are competing reactions. Reactions 1 and 2 are not meant to be pitted against each other, but to explain the different microstructures 1 and 2, which potentially arise due to the different availability of K.

MC: As additional information, we now state the composition of recrystallized feldspar and also the fact that recrystallization was dynamic.

---

10) *There is a claim of "coeval development" of a (synkinematic?) dry assemblage and a wet one in the same rock with reference to S5. But the figure in S5 only shows a dry assemblage, and it is a static texture (could that be Musgravian even?).*

AC: The static microstructural overprint in S5 is consistent with the observations made in other deformed and undeformed samples which have been overprinted during the Petermann Orogeny. We agree that the appendix figure was actually more confusing than helpful to the reader, which is why we dropped it.

MC: Appendix S5 and its respective reference in the manuscript have been omitted.

---

11) *The claim that fluid activity has been "quantified" is not justified; this is a qualitative evaluation, not a quantitative one. However, there is still a convincing case that there was indeed more water in the north than in the south; but the case is currently overstated in terms of what has really been constrained petrologically.*

AC/MC: A valid point: we have replaced "quantified" with "estimated", reflecting the fact that the estimations are only qualitative.

---

12) *Lines 75-80: What is the significance of these earlier mylonites?*

AC: We included these earlier mylonites for the sake of keeping the geological history complete. However, we agree that this is only confusing to the reader. The mylonites are described in more detail in Wex et al. (2017), but are not relevant to the current manuscript.

MC: The mentioning of the earlier mylonites has been omitted from the manuscript, because they are not relevant here and were not further discussed.

---

13) *Lines 90-95: Two stages of deformation and P-T conditions are given, but only one long set of "stable" mineral assemblages is given. Stable with respect to which stage?*

AC: We agree that this aspect is confusing to the reader. As discussed in comment 5), the mentioned two stages of deformation are irrelevant to the current paper, which is why only a single list of minerals, those stable during the Petermann Orogeny, is given. Since the mentioning of the two stages has now been dropped, a single list of minerals is sufficient.

_____

14) *Section 5.1: Can an estimated error be quoted for the Th measurements?*

AC/MC: Measurements were run until the error was < 10% (stated in appendix S1). We now provide this information also in the manuscript.

_____

15) *Line 187: switch 6 ppm and 8 ppm*

AC/MC: done.

_____

16) *Fig. 4: how is the lower bound of the mylonite zone defined and how well is that constrained?*

AC: The lower bound of the mylonite zone is defined by the initial appearance of Petermann mylonitic foliation well characterized by the trend of the stretching lineation and by the top-to-north kinematic indicators. Due to the gradual and irregular nature of the mylonite zone, with high-strain shear zones surrounding less to little deformed low-strain domains on the metre- to kilometre-scale, the lower bound is less well defined than its upper counterpart, but on the whole still reliable.

MC: The information that the lower bound is defined by the initial appearance of mylonites with Petermann kinematics is now provided.

_____

17) *Fig. 5: Airborne Th maps – how sensitive is this measurement to depth? What is the thickness of the Kelly Hills klippe? Could that be a contributor to increased Th signal?*

AC: As stated by Jones and Schreib (2007): "The gamma ray signal for natural radioisotopes in rocks comes almost entirely from the top 35 cm (IAEA, 2003)", thus making the thickness of the Kelly Hilly klippe irrelevant to the increased Th signal.

D G JONES AND C SCHEIB. 2007. A preliminary interpretation of Tellus airborne radiometric data. British Geological Survey Commissioned Report, CR/07/061. 70pp.

IAEA. 2003. Guidelines for radioelement mapping using gamma ray spectrometer data. International Atomic Energy Agency IAEA-TECDOC, 1363, pp. 173.

MC: This clarification, together with the references, has now been added.

_____

18) *Line 207: Why assume all PST is in the hanging wall?*

AC: We did not want to give the impression that pseudotachylytes were exclusively restricted to the hanging wall, since this is clearly not true. However, it is evident from field observations that the largely unsheared pseudotachylyte breccias in the hanging wall are locally sheared and dragged into the Woodroffe Thrust mylonitic zone.

MC: The statement has been reformulated into: "Similar field relationships, such as progressive downwards mylonitization of units clearly forming part of the hanging wall, also indicates limited reworking of the Fregon Subdomain at locations 4 and 6 (Fig. 5)".

_____

19) *Section 6.2: indicate whether these measurements are in interpreted hanging wall or footwall*

AC/MC: This information is now provided in the Appendix Table S1.

_____

20) *Section 7: why do this only on the PST? Why not directly on the host rocks?*

AC: Pseudotachylytes have been identified as preferred discontinuities for nucleation of shear zones under mid- to lower crustal conditions.

MC: This concept is now included at the beginning of section 7 with an extensive list of supporting references.

---

21) *Fig. 9 – not needed*

AC/MC: Fig. 9 has been deleted.

---

22) *Line 320: Na is not considered either. Iron could also come from Bt or garnet.*

AC/MC: The equations presented are indeed very simplified but are only taken as indicative of the reactions involved. Biotite and garnet have been added as potential sources of iron.

---

23) *Fig. 8 and 10 – where does the regional temperature gradient come from and what is its interpreted meaning?*

AC: This aspect is discussed in comments 3) and 6).

MC: Additional information on how Wex et al. (2017) constrained the syn-kinematic P-T conditions and the interpreted meaning of these values has been added.

---

24) *Line 360 – did not quantify water activity*

AC: We have replaced "quantified" with "estimated".

---

25) *Section 8.3.2 – this all supports an external fluid source; so how to reconcile?*

AC: Our data does not allow us to reconcile towards a single fluid source. Our observations and results indicate that the H_2O and CO_2 each originated from different sources. We argue in favour of an internal source for the hydrous fluids, whereas the fact that we observe syn-kinematic calcite growth in otherwise non-carbonaceous rocks clearly indicates that carbon was introduced externally. Additional stable isotopic analysis on calcite, unfortunately, did not provide any significant constraints, allowing no further conclusions to be drawn without speculation.

MC: The interpretation of the isotopic analysis have been shifted entirely into the appendix with only a short summary of the isotopic results provided in the main manuscript. The potential mantle source as the most likely source has been dropped. The different possibilities are still presented in the appendix, however we reconcile by not trying to over interpret our isotopic results, since they are simply not conclusive enough.

---

26) *Line 422-23: distinguish "water weakening" from simply a rheologically weaker assemblage (e.g., higher mica abundance?)*

AC/MC: done.

---

27) *Line 437: this also argues against a "closed system"*

AC: We agree that our argumentation, that the generally low abundance of hydrous minerals in both hanging wall and footwall in the "dry" southern locations potentially promoted a similar rheological response in both units, is indeed rather speculative. It is, in fact, also not supported by our Table 4.

MC: We decided to drop the mentioned statement and now solely argue that the local reworking of the lowermost hanging wall was guided by the presence of pseudotachylyte.

---

28) *Line 450-451: clarify why increasing fluid-rock interaction would result in volume loss?*

AC: We admit that there is no evidence for volume loss associated with fluid-rock interaction.

MC: The statement is omitted in the new manuscript version.

Author Comment (AC) and manuscript changes (MC) on interactive comment by F. Fusseis

(florian.fusseis@ed.ac.uk)

1) *First, I find it curious that the authors miss the opportunity to discuss the significant increase in shear strain due to the narrowing of the Woodroffe thrust from south to north in light of the strain softening mechanisms they envisage. The relatively lapidary last sentence of the discussion (line 463) does, in my eyes, not explain why the Woodroffe thrust is six-fold narrower in the north, especially if the wetter conditions do not account for the pronounced strain localization there. The observation that the thrust narrows so dramatically would invite a more detailed discussion of the microstructural developments along the strain gradients in the north and south, or, in other words, the strain-dependent evolution of the mylonites. Which mechanisms accommodate strain softening in the north and south? Is it possible that the shear zone progressively narrowed during shearing, in analogy with Means' (1995) type 2 shear zones? If so, does this apply to the entire Woodroffe thrust? And if not, why not? I would invite the authors to include a more detailed microstructural description of the evolution from host rock to ultramylonite in both, northern and southern sections, and then integrate these into the discussion of their findings in light of the questions above.*

AC/MC: After reconsideration, we agree with the reviewer that our previous conclusion that the narrowing is exclusively controlled by temperature is probably too restrictive and not justified. The last sentence of the discussion has therefore been extended into a more detailed discussion on the potential role of aqueous fluids as an additional or alternative explanation for the narrowing of the Woodroffe Thrust from south to north. We have updated the discussion to argue that an increase in the water content to the north would potentially result in an increase of the effective viscosity ratio between footwall and hanging wall, potential causing a stronger localization toward the interface and a narrower mylonite zone that extends less into the stronger material. Indeed, we envision a progressive narrowing of the Woodroffe Thrust with time, in analogy with Means' (1995) type 2 shear zones. Microstructural and petrological evidence for this is found in the southern outcrops of the Woodroffe Thrust, with the temporal development in detail discussed by Wex et al. (2017). A detailed discussion of the microstructural developments along the strain gradients in the north and south, as requested by the reviewer, has been carried out in the overall framework of our study of the Woodroffe Thrust, but has been drafted into a follow-up companion paper, which focuses particularly on the microstructural gradients parallel to the thrusting direction and the inferred deformation mechanisms in quartz and feldspar, as characteristic for middle to lower continental crust.

---

2) *Second, the mantle source of the CO2-dominated brines. If these are indeed mantle-derived, how did they migrate along the shear zone? Was there some form of synkinematic porosity? If there was a fluid migrating along the Woodroffe thrust, what was its micromechanical effect in both, the northern and southern sections?*

AC/MC: There is no indication that there is preferentially more calcite in the more strongly mylonitic to ultramylonitic rocks, arguing against channeling of the CO_2-rich fluids along the Woodroffe Thrust. Furthermore, we agree that the whole calcite isotope story is not conclusive, and our current conclusions based on this data slightly overambitious. The interpretation of the calcite isotopic data has been formulated into more restrained statements and is, in the revised manuscript, restricted to the appendix. A short summary of the isotopic results is still provided in the main manuscript.

---

3) *With respect to the determination of the modal abundance of the hydrous minerals (S1.3) – global thresholding on the basis of grey value histograms is rather primitive and prone to substantial errors – Fiji/ImageJ offers much more sophisticated segmentation algorithms, in particular trainable WEKA segmentation, a machine learning toolbox.*

AC: The FiJi/ImageJ software does provide more sophisticated segmentation tools but it also requires careful checking of the output results. We put particular care in checking that the greyscale histograms

of the collected SEM images allowed a clear separation between the hydrous minerals and the anhydrous minerals. We believe that the determined modal abundance of hydrous minerals with our thresholding technique is quite reliable.

Inverted distribution of ductile deformation in the relatively "dry" middle crust across the Woodroffe Thrust, central Australia

Sebastian Wex[1], Neil S. Mancktelow[1], Friedrich Hawemann[1], Alfredo Camacho[2], Giorgio Pennacchioni[3]

[1]Department of Earth Sciences, ETH Zurich, Sonneggstrasse 5, 8092 Zurich, Switzerland
[2]Department of Geological Sciences, University of Manitoba, 125 Dysart Rd, Winnipeg, Manitoba, R3T 2N2, Canada
[3]Department of Geosciences, University of Padova, Via Gradenigo 6, 35131 Padova, Italy

Correspondence to: Neil S. Mancktelow (neil.mancktelow@erdw.ethz.ch)

Abstract. Thrust fault systems typically distribute shear strain preferentially into the hanging wall rather than the footwall. ~~In this paper, we present~~The Woodroffe Thrust in the Musgrave Block of central Australia is a regional-scale example that does not fit this model. ~~The Woodroffe Thrust~~ It developed due to intracontinental shortening during the Petermann Orogeny (ca. 560-520 Ma) ~~in central Australia. It~~and is interpreted to be at least 600 km long in its ~~general~~ E-W strike direction, with an approximate top-to-north minimum ~~relative~~ displacement of 60-100 km. The associated mylonite zone is most broadly developed in the footwall. The immediate hanging wall was only marginally involved in the mylonitization process, as can be demonstrated from the contrasting thorium signatures of mylonites derived from the upper amphibolite facies footwall and the granulite facies hanging wall protoliths. Thermal weakening cannot account for such an inverse deformation gradient, as syn-deformational P-T estimates for the Petermann Orogeny in the hanging wall and footwall from the same locality are very similar. The distribution of pseudotachylytes, which ~~act~~acted as preferred nucleation sites for shear deformation, also cannot provide an explanation, since these fault rocks are especially prevalent in the immediate hanging wall. The most likely reason for the inverted deformation gradient across the Woodroffe Thrust is water-assisted weakening due to the increased, but still limited, presence of aqueous fluids in the footwall. ~~On the contrary, the presence or absence of aqueous fluids does not appear to be linked to the regional variation in mylonite thickness, which generally increases with increasing metamorphic grade.~~ We also infer that the relative increase of fluids in the footwall in the direction of thrusting, together with the slight decrease in the temperature of mylonitization (ca. 100 °C), was responsible for the observed 6-fold decrease in thickness (from ca. 600 m to 100 m) of the Woodroffe Thrust mylonitic zone.

1 Introduction

Continental fault and shear zone systems with displacements on the order of several tens to hundreds of kilometres generally show an asymmetric mylonite distribution across the main fault horizon that is opposite for reverse faults or thrusts and normal faults or detachments. Fault zones are predicted to become more viscous and broaden with depth (e.g., Fossen and Cavalcante, 2017; Handy et al., 2007; Mancktelow, 1985; Passchier and Trouw, 2005; Platt and Behr, 2011b). Juxtaposition of initially different crustal levels should therefore result in a geometry that, for a thrust, preferentially preserves the broader ductile

mylonite zone in the hanging wall, whereas, for a detachment, it should be in the footwall ~~(e.g., Mancktelow, 1985, his Fig. 11). This model is valid for many large-scale fault systems, for example:~~(e.g., Mancktelow, 1985, his Fig. 11; Passchier, 1984, his Fig. 2). This model is valid for many large-scale fault and shear zone systems, for example: the Moine Thrust Zone, NW Scotland (Christie, 1963; Coward, 1980), the Alpine Fault, New Zealand (Cooper and Norris, 1994; Sibson et al., 1981), the Saint-Barthélemy Massif shear zone (Passchier, 1984), the Simplon Fault, central European Alps (Mancktelow, 1985), the ~~Alpine Fault, New Zealand (Cooper and Norris, 1994; Sibson et al., 1981), the Grizzly Creek shear zone, Colorado (Allen and Shaw, 2011)~~Grizzly Creek shear zone, Colorado (Allen and Shaw, 2011) and the Whipple mountains detachment fault, ~~southwestern~~south-western U.S. (Davis, 1988; Davis and Lister, 1988). The ~~miderustal~~mid- to lower crustal Woodroffe Thrust of central Australia (Major, 1970) is an example that does not fit this model and predominantly developed a broader mylonite zone in the footwall (Bell and Etheridge, 1976; Camacho et al., 1995; Flottmann et al., 2004). An interpretation of the Woodroffe Thrust as an original detachment that was later re-oriented and exploited as a thrust can be excluded, both because the metamorphic grade decreases in the direction of tectonic transport and because field mapping shows that the fault zone steepens and ramps down towards the internal part of the orogen, against the transport direction (Wex et al., 2017). Passive transport and thermal weakening also cannot account for the inverse deformation gradient, as there is no evidence for late brittle movement on the thrust plane and syn-deformational P-T estimates in the hanging wall and footwall from the same locality are very similar (Wex et al., 2017). Bell and Etheridge (1976) and Camacho et al. (1995) proposed that the inverted distribution of ductile deformation is explained by the difference in bulk water content between the upper amphibolite facies (1.0 wt%) footwall and the granulite facies (0.2 wt%) hanging wall, reflecting the metamorphic conditions in the protolith prior to thrusting. Similarly, the preferential formation of shear zones in regions where the host rock mineralogy had previously been modified by fluid-rock interaction has, for example, also been documented in the Whipple mountains detachment fault in SE California (Selverstone et al., 2012) and the Neves area of the Tauern Window in the eastern Alps (Mancktelow and Pennacchioni, 2005). In this paper, we ~~quantify~~discuss the control of host rock lithology and ~~potential~~, potentially, of fluid activity on the distribution of ductile deformation across the Woodroffe Thrust, in an attempt to critically test the local findings of Bell and Etheridge (1976) ~~from the Amata area (western edge of Fig. 1)~~and Camacho et al. (1995) on a more regional scale (Fig. 1). We also investigate the effect of varying metamorphic temperatures and fluid conditions on the variation in mylonite thickness over a distance of ca. 60 km parallel to the direction of thrusting.

2 Geology

The mid- to lower crustal ~~scale~~ Woodroffe Thrust outcrops in the Musgrave Block of central Australia (Major, 1970) ~~is developed over an approximate E-W strike length generally interpreted to exceed 600 km. It separates the Mulga Park Subdomain in the footwall from the Fregon Subdomain in the hanging wall (Edgoose et al., 1993; Major and Conor, 1993). Exposure of the Woodroffe Thrust is poor to inexistent in the~~are located within the suture zone of the north, west, and south Australian cratons, which amalgamated into the Australian continent at ca. 1300 Ma in an early stage of development of the

supercontinent Rodinia (Myers et al., 1996). The Woodroffe Thrust is developed over an E-W strike length generally interpreted to exceed 600 km and separates the Mulga Park Subdomain in the footwall (to the north) from the Fregon Subdomain in the hanging wall (to the south) (Camacho and Fanning, 1995; Edgoose et al., 1993; Major and Conor, 1993). Exposure of the thrust is poor to inexistent in its proposed western (e.g., Stewart, 1995, 1997) and eastern (e.g., Edgoose et al., 2004) prolongations, but is generally excellent for ca. 150 km in the central Musgrave Block (Bell, 1978; Camacho et al., 1995; Collerson et al., 1972; Wex et al., 2017), where the current study was conducted. In this region, both footwall and hanging wall predominantly consist of granitoids (more common in the footwall) and quartzo-feldspathic gneisses (more common in the hanging wall), with subordinate metadolerites, mafic gneisses and metapelites (Fig. 1). Rare quartzites, amphibolites and schists are restricted to the footwall (Camacho and Fanning, 1995; Collerson et al., 1972; Major, 1973; Major and Conor, 1993; Scrimgeour and Close, 1999; Young et al., 2002). Protoliths are inferred to have been felsic volcanics, sediments and intrusives with depositional or emplacement ages around ca. 1550 Ma (Camacho, 1997; Camacho and Fanning, 1995; Gray, 1977, 1978; Gray and Compston, 1978; Maboko et al., 1991; Major and Conor, 1993; Sun and Sheraton, 1992). These ~~rocks~~protoliths were regionally

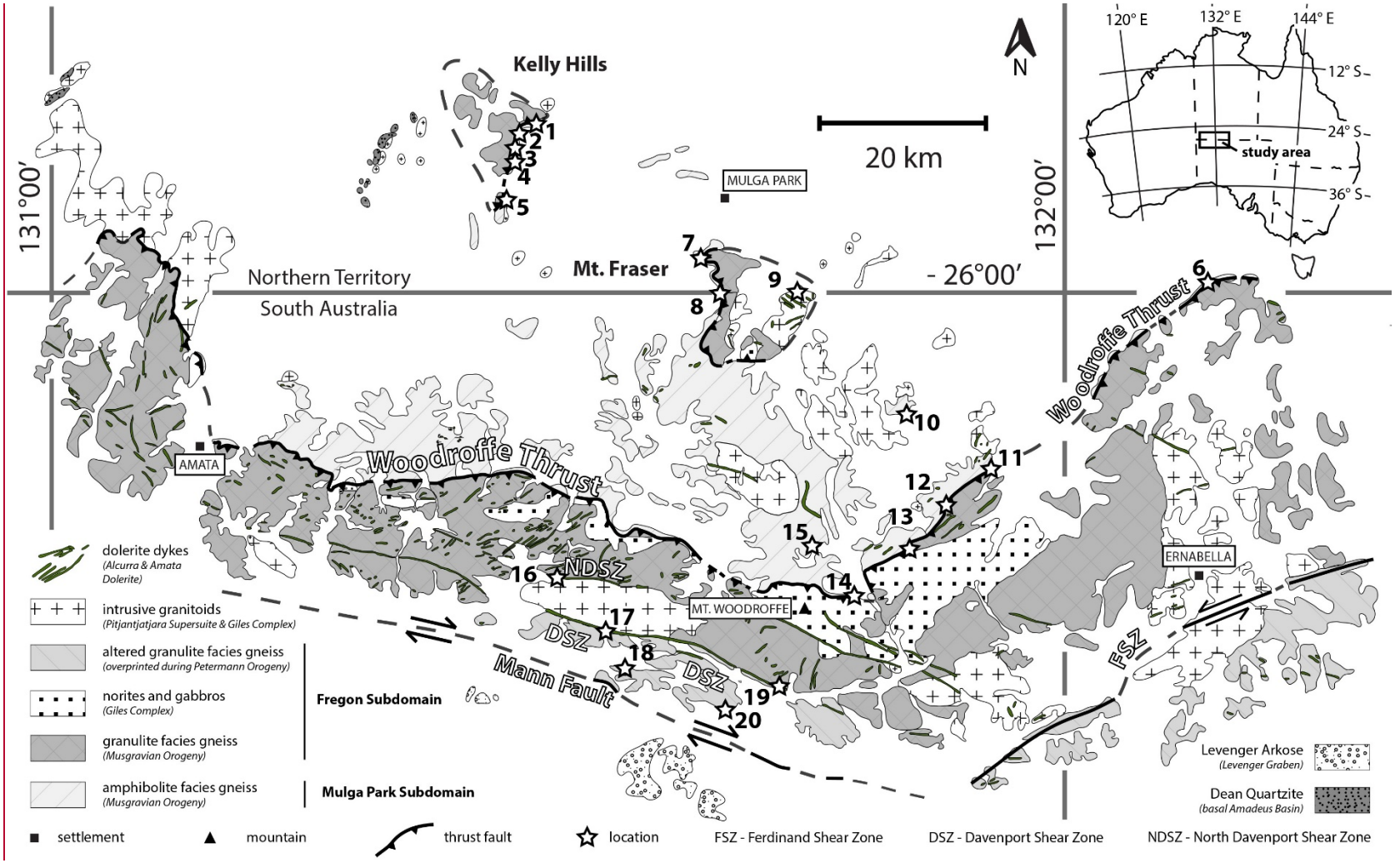

Figure 1: Geological map of the central Musgrave Block (modified after Major et al., 1967; Sprigg et al., 1959; Young et al., 2002).

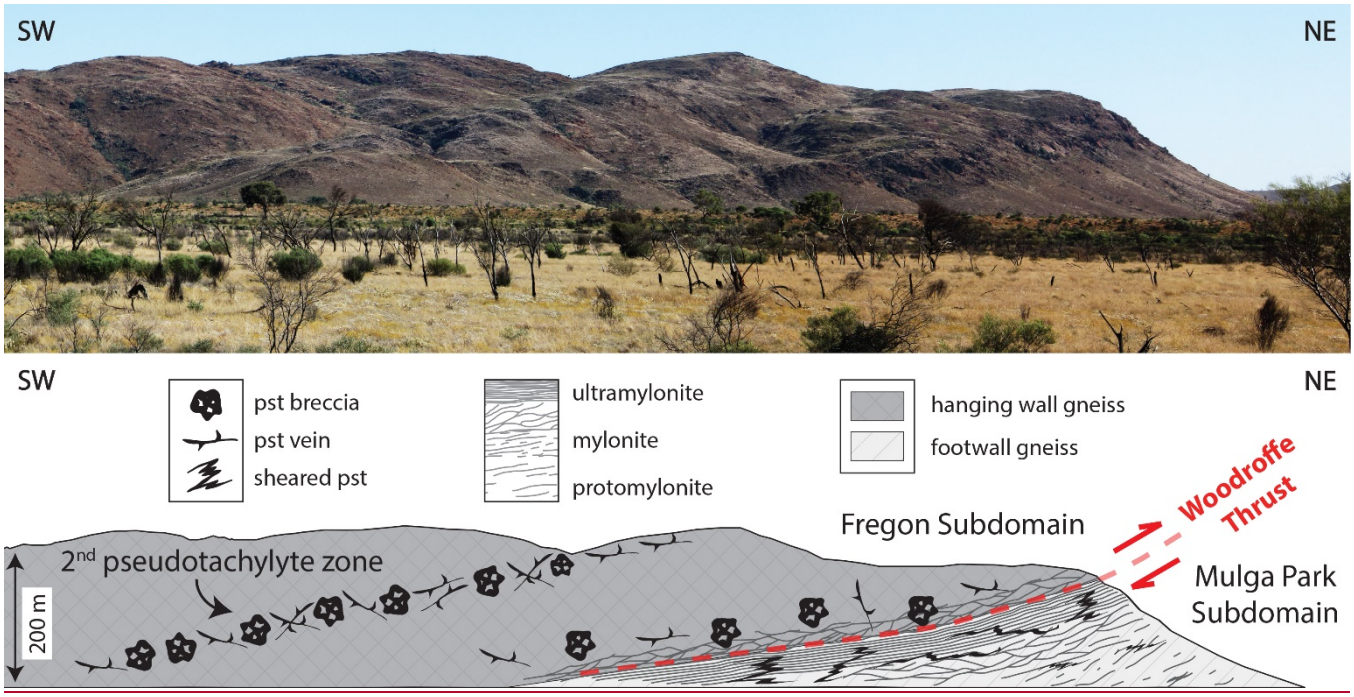

Figure 2: Photograph and schematic sketch of a cross section through the Woodroffe Thrust at Kelly Hills. Ductile deformation is almost entirely ~~localized~~concentrated in the immediate footwall (Mulga Park Subdomain), developing a sequence of protomylonites, mylonites and ultramylonites, with the degree of mylonitization decreasing into the footwall. In contrast, the mostly unaffected or only weakly foliated hanging wall (Fregon Subdomain) is characterized by ubiquitous and voluminous pseudotachylyte (pst) veins and breccias. Further into the hanging wall, a dip slope, characterized by a second zone of highly abundant unsheared pseudotachylyte, has also been documented. Photograph coordinates: 131.45077, -25.89823.

deformed and metamorphosed ~~into~~at upper amphibolite facies (Mulga Park Subdomain) to granulite facies (Fregon Subdomain) ~~gneisses~~conditions during the ca. 1200 Ma Musgravian Orogeny (Camacho, 1997; Camacho and Fanning, 1995; Gray, 1978; Maboko et al., 1991; Sun and Sheraton, 1992), and syn- to ~~posttectonically~~post-tectonically intruded by the Pitjantjatjara Supersuite granitoids between ca. 1170-1130 Ma (Camacho, 1997; Camacho and Fanning, 1995; Scrimgeour et al., 1999; Smithies et al., 2011). ~~Subsequently~~Peak temperature and pressure conditions during the Musgravian Orogeny are controversial. Earlier estimates were ca. 820-900 °C and 1.1-1.4 GPa (Ellis and Maboko, 1992; Maboko et al., 1989, 1991) but more recent studies have given conditions of ca. 800-1000°C and 0.6-0.9 GPa (Camacho, 1997; Tucker et al., 2015; Walsh et al., 2015). Subsequent to this regional-scale tectono-metamorphic phase, the area experienced bimodal magmatism (Giles Complex, including the Alcurra Dolerite swarm) between ca. 1080-1050 Ma and mafic magmatism (Amata Dolerite) at ca. ~~800 Ma (Ballhaus and Glikson, 1995; Camacho et al., 1991, 1997; Clarke et al., 1995; Edgoose et al., 1993; Sun et al., 1996; Zhao et al., 1994; Zhao and McCulloch, 1993).~~800 Ma (Ballhaus and Glikson, 1995; Camacho et al., 1991; Clarke et al., 1995;

Edgoose et al., 1993; Evins et al., 2010; Schmidt et al., 2006; Sun et al., 1996; Zhao et al., 1994; Zhao and McCulloch, 1993).

In the area considered in the current study, ~~large Giles Complex gabbro-norite intrusions are restricted to the Fregon Subdomain. In parts of the field area (locations 11-13 in Fig. 1), mylonites with top-to-west kinematics, postdating the emplacement of dolerite dykes but preceding the main Woodroffe Thrust mylonites, have been recognized but remain largely undocumented (Wex et al., 2017). Aside from this local deformation phase, the central Musgrave Block remained virtually~~gabbro-norite intrusions, correlated to the Giles Complex, are restricted to the Fregon Subdomain. Except for these periods of magmatic intrusion, the central Musgrave Block remained largely unaffected by tectonic events between the Musgravian Orogeny at ca. 1200 Ma and the Petermann Orogeny at ca. 560-520 Ma

Figure 3: Sharp contact between the ultramylonites of the Woodroffe Thrust (below ~~dashed line~~) and the largely undeformed felsic granulite in the hanging wall (above ~~dashed line~~). Photograph looking perpendicular to the direction of thrusting. Outcrop SW13-135 (coordinates: 131.87939, -26.21188; location 12 in Fig. 1).

(Camacho and Fanning, 1995; Maboko et al., 1992). Earlier studies by Maboko et al. (1989; 1991) and Ellis and Maboko (1992) proposed that the Musgravian and Petermann Orogenies represented successive stages of a single counterclockwise P-

T-t path, whereas Camacho (1997) and Camacho et al. (1997; 2015) suggested that the Musgrave Block was partially exhumed prior to the onset of the Petermann Orogeny and then reburied.

The Petermann Orogeny produced a number of large-scale mylonitic shear zones, amongst which the Woodroffe Thrust is the most prominent. Ductile deformation during top-to-north thrusting along the Woodroffe Thrust was largely accommodated ~~in~~within the Mulga Park Subdomain footwall (Bell and Etheridge, 1976; Camacho et al., 1995; Flottmann et al., 2004) and is characterized by mylonites with varying degrees of strain, ranging from protomylonites to ultramylonites (Fig. 2), anastomosing around low-strain domains on the metre- to kilometre-scale. ~~These mylonites preserve an annealed and a non-annealed microstructure, interpreted to record lower crustal (ca. 650 °C and 1.0-1.3 GPa) and midcrustal (ranging from ca. 520-620 °C and 0.8-1.1 GPa) shearing stages of the Woodroffe Thrust~~The syn-kinematic conditions of deformation along the Woodroffe Thrust were constrained by conventional geothermobarometry to be within the range of 520-650 °C and 0.8-1.3 GPa (Wex et al., 2017) and thus lower grade when compared to peak conditions during the earlier Musgravian Orogeny. The metamorphic assemblage in both mylonitic samples (where the metamorphic aggregate developed syn-kinematically) and in statically overprinted undeformed samples (e.g. some Alcurra and Amata Dolerite dykes) record similar metamorphic conditions, consistent with ambient mid- to lower crustal levels ~~(Wex et al., 2017).~~(Wex et al., 2017). Stable mineral assemblages during the Petermann Orogeny in felsic units of the Woodroffe Thrust comprise (decreasing modal abundance from left to right) Qz + Pl + Kfs + ~~Grt +~~ Bt + Ilm ± Grt ± Ep ± Ms ± Ky ± Cpx ± Hbl ± Rt ± Ttn ± Mag ± Cal, whereas mafic units consist of Pl + Ilm ± Cpx ~~+~~± Grt~~ + Ilm~~ ± Rt ± Opx ± Bt ± Hbl ± Ky ± Mag ± Qz ± Kfs ± Cal (Wex et al., 2017). Mineral abbreviations are after Whitney and Evans (2010). The degree of mylonitization progressively decreases into the footwall but shows a very abrupt transition into the immediate, dominantly brecciated hanging wall (Figs. 2, 3), which is characterized by ubiquitous and voluminous pseudotachylyte veins and breccias (Camacho et al., 1995; Lin et al., 2005). Even though this upper boundary of the mylonites is discrete or rapidly transitional in the field (Fig. 3), it does not necessarily represent the original boundary between the Mulga Park (footwall) and Fregon (hanging wall) Subdomains. In the Amata area (western edge of Fig. 1), Bell (1978) reported up to 250 m of marginal hanging wall reworking into the mylonite zone. However, it remains uncertain how this value was exactly determined, since hanging wall and footwall mylonites are very similar in their field appearance.

3 Methods and general approach

The hanging wall, footwall and numerous transects across the Woodroffe Thrust have been studied and sampled ~~at the~~along a N-S traverse, parallel to the direction of thrusting. The sampling locations are reported in Fig. 1. Thin sections of the sampled mylonites were prepared from rock chips cut perpendicular to the foliation and parallel to the stretching lineation, and analysed using standard polarized light and scanning electron microscopy. Firstly, the distribution of ductile deformation along and across the Woodroffe Thrust was characterized by quantifying (1) the regional variation in the maximum thickness of the mylonitic zone and (2) the associated degree of hanging wall and footwall reworking. Secondly, field and thin section

observations were compiled to assess in a qualitative manner (3) the presence/absence of ~~aqueous~~ fluids during deformation, and (4) the regional variability in modal abundance of hydrous minerals in felsic units. Potential correlations between parameters (1) to (4) are then discussed. Sample/outcrop coordinates are given in the world geodetic system (WGS) 1984. Orientation measurements of structural elements are corrected for magnetic declination. A detailed description of all utilized methods is given in the Supporting Information S1.

4 Mylonite thickness

Field observations indicate that the thickness of the Woodroffe Thrust mylonites is variable. In a section perpendicular to strike, the thickness (*T*) of the mylonitic zone across the Woodroffe Thrust was calculated by trigonometry (Fig. 4) from: (i) the angle of dip (α) of the thrust (measured in the field and averaged for each transect); (ii) the respective difference in elevation (*p*) (derived from the 30x30 m digital elevation model ASTER) between the lower and upper structural boundaries of the mylonites to the unsheared country rocks (determined from field observations and remote sensing); and (iii) the apparent thickness (*q*) (derived from remote sensing). The upper boundary of the mylonitic zone is easily recognized (Fig. 3~~), whereas the~~). The lower boundary is ~~generally less~~determined by the first appearance of Petermann mylonitic foliation, well ~~defined due to its gradual~~characterized by the approximate N-S trend of the stretching lineation and ~~irregular nature (Fig. 2), with high-strain shear zones surrounding less to little deformed low-strain domains on the metre- to kilometre-scale.~~by the top-to-north kinematic indicators. Errors for parameters α and *q* are considered negligible, whereas the 30x30 m resolution of the digital elevation model is prone to introduce an uncertainty on the order of 10-20 m. The geometrical arrangement for the estimate of *T* was the same for locations 2-8 and 12-14 (Fig. 4a), but slightly different for location 11 (Fig. 1), where the lower structural boundary of the mylonites was at a higher elevation than the upper boundary (Fig. 4b). The thickness of the mylonitic zone at location 1 (Fig. 1) was not calculated, because the Woodroffe Thrust is only exposed along strike. The results for all other studied transects are summarized in Table 1 and, independent of local variability, indicate a gradual increase in mylonite thickness from ~~the northern locations 2-8 (average 120 m) via the central locations 11-12 (ca. 300 m) to the southern locations 13-14 (ca. 600 m).~~ca. 100 m in the north to ca. 600 m in the south.

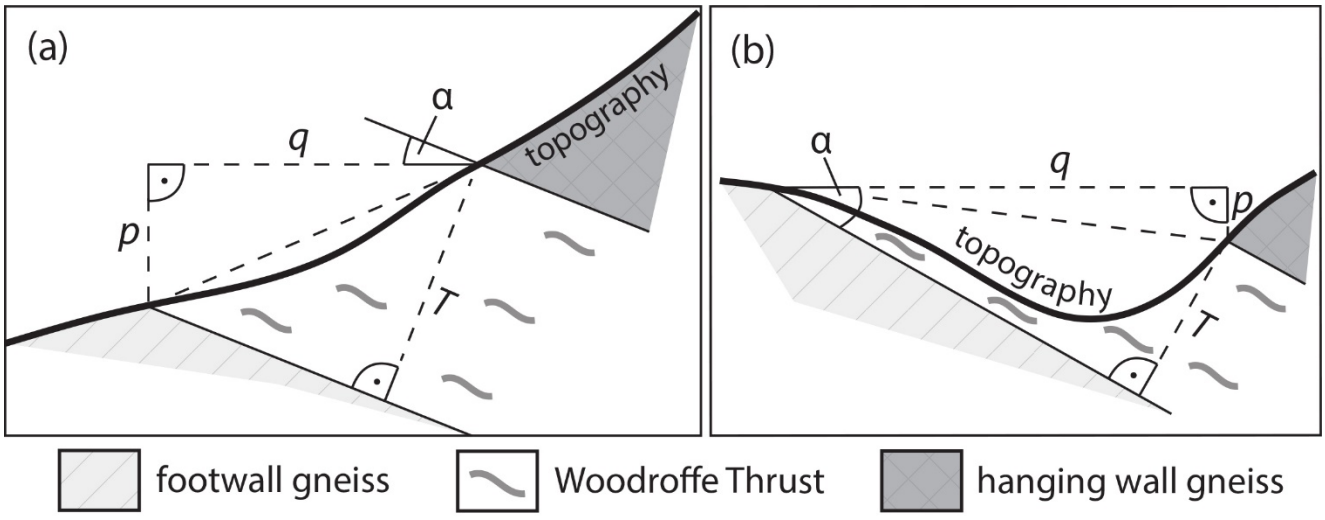

Figure 4: Schematic illustration of the trigonometry applied to quantify the true thickness of the Woodroffe Thrust mylonitic zone in a section perpendicular to strike. The parameters are defined in the main text. (a) Geometry applicable to locations 2-8 and 12-14 of Fig. 1. (b) Geometry applicable to location 11 of Fig. 1.

location	coordinates (WGS 1984)		trigonometrical parameters			
(Fig. 1)	longitude	Latitude	α (°)	*p* (m)	*q* (m)	*T* (m)
2	131.454	-25.845	27	22	150	88
3	131.452	-25.855	43	54	190	169
4	131.449	-25.873	36	23	160	113
5	131.442	-25.904	21	44	130	88
6	132.143	-25.992	29	62	160	132
7	131.644	-25.963	17	110	250	178
8	131.663	-25.999	10	60	130	82
11	131.926	-26.177	28	61	800	322
12	131.879	-26.212	24	153	430	315
13	131.844	-26.253	37	124	850	611
14	131.774	-26.308	25	128	1200	623

Table 1: Angle of dip (α), elevation difference (*p*), apparent thickness (*q*) and true thickness (*T*) of the Woodroffe Thrust mylonites in the central Musgrave Block.

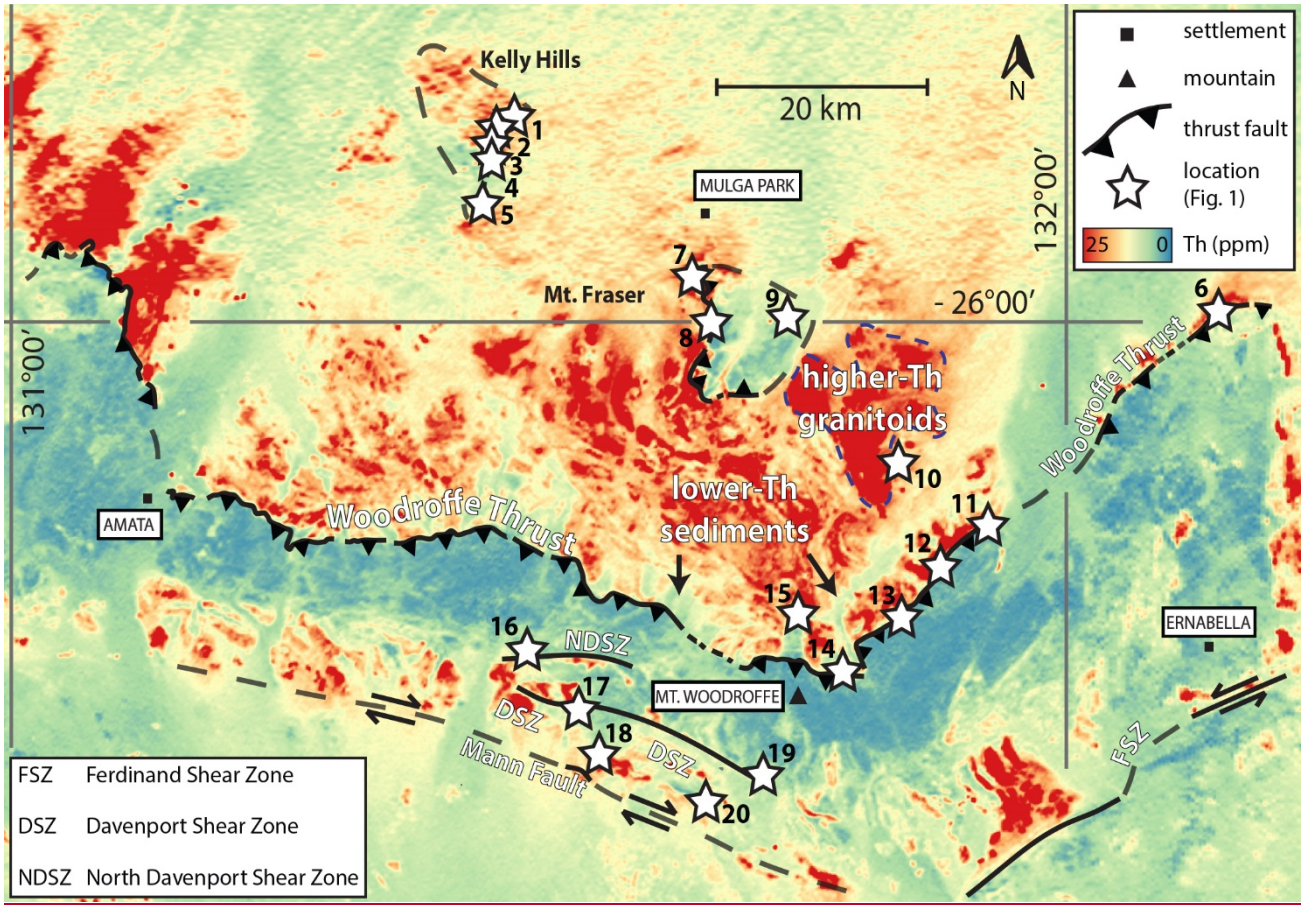

Figure 5: Airborne thorium (ppm) map of the central Musgrave Block. Data derived from the Australian Geophysical Archive Data Delivery System (GADDS) under www.ga.gov.au/gadds (Percival, 2010). The hanging wall Fregon Subdomain is generally depleted compared to the footwall Mulga Park Subdomain. Granitoid intrusives of the Pitjantjatjara Supersuite often have higher-thorium content, particularly in the footwall (one example surrounded by the blue dashed ~~lines~~line), but also in the southern part of the hanging wall. Lower-thorium signatures forming diffuse tongues extending northward into the footwall are attributed to alluvial wash derived from the hanging wall. The distinction in thorium content is no longer evident for the northernmost klippe of the hanging wall in the Kelly Hills area (locations 1-5) and the northernmost part of the Mt. Fraser klippe (location 7).

5 Degree of hanging wall and footwall mylonitization

Mylonites derived from the hanging wall and footwall of the Woodroffe Thrust are very similar in both their field appearance and microstructural-petrographical characteristics. The high degree of recrystallization and general lack of porphyroclasts in the uppermost mylonites at locations 4, 6-8 and 12-14 (Fig. 1) ~~suggests~~suggest that these samples were potentially derived from the pseudotachylyte-rich Fregon Subdomain, hence indicating local hanging wall reworking. To establish whether mylonites were derived from either the Mulga Park or the Fregon Subdomains, we utilized their thorium concentrations, based

on the general observation that hanging wall rocks are depleted in thorium compared to footwall rocks (Fig. 5). This contrast is due to (1) dehydration and melting reactions during the earlier ca. 1200 Ma Musgravian Orogeny, which depleted the granulite facies hanging wall to a greater degree than the upper amphibolite facies footwall (Heier and Adams, 1965; Lambert and Heier, 1967, 1968), (2) the predominance of granitoids rather than gneisses in the footwall, and (3) the fact that low-thorium Giles Complex gabbro-noritic intrusions are ~~often~~commonly exposed in the immediate hanging wall of the Woodroffe Thrust. Deformation and metamorphism during mylonitization did not significantly alter the original thorium content of the rocks, since the thorium-bearing phases, such as zircon, allanite, monazite and apatite did not break down during the Petermann Orogeny. Consequently, the original variation in thorium between the granulite and amphibolite facies rocks was preserved (Fig. 5). Anomalies in this broad pattern are present locally and can be attributed to hanging wall-derived alluvial sediments in the immediate footwall (lower-thorium anomaly) and to granitoid intrusions of the Pitjantjatjara Supersuite ~~and Giles Complex~~ (higher-thorium anomaly), which are syn- to post-Musgravian upper amphibolite to granulite facies metamorphism (Scrimgeour and Close, 1999; Young et al., 2002) (Fig. 5). The contrast between a lower-thorium hanging wall and a higher-thorium footwall is well-defined on the airborne thorium map for the central and southern locations ~~6, 8 and 11-14~~, but less evident in the ~~northern locations 1-5 and 7~~north (Fig. 5). Thorium measurements were carried out on thin section chips of felsic gneisses and granitoids via γ-ray spectrometry~~.~~, with the measurements run until the error (2 x standard deviation) was below 10 %. The method is outlined in detail in the Supporting Information S1.

5.1 Thorium concentration in felsic units

Thorium contents of felsic gneisses and granitoids (Table 2) have been compiled from the current study as well as from previous studies of nearby areas (Camacho, 1997; Young et al., 2002). These data have been grouped into (1) the central and southern locations ~~(6, 8, and 11-14)~~ and (2) the northern locations ~~(1-5, and 7),~~, based on the airborne thorium map, as introduced above.

In group (1), samples unequivocally attributed to either the hanging wall or footwall of the Woodroffe Thrust were grouped together. This was done on the basis of their geographical position, with respective samples originating either from far into the non-mylonitized hanging wall and footwall or from the lowermost protomylonitic part of the Woodroffe Thrust. In the hanging wall, thorium concentrations range from 1 to 28 ppm in felsic gneisses and up to 63 ppm in granitic intrusions (higher-thorium anomalies), but are in both cases usually lower than 8 ppm. In the footwall, concentrations vary between 2 and 195 ppm and are typically higher than 10 ppm (Table 2). These concentrations are in accord with the regional-scale contrast in thorium concentrations across the Woodroffe Thrust in the central and southern locations ~~6, 8 and 11-14~~ (Fig. 5), as well as with the results of Lambert and Heier (1968), who determined concentrations of 2.1 ppm for the granulite facies hanging wall and 11 ppm for the upper amphibolite facies footwall. Based on the compilation in Table 2, samples with thorium content <8 ppm were assigned to the hanging wall and samples with higher values to the footwall of the Woodroffe Thrust. ~~Five different transects were investigated (locations 8 and 11-14 in Fig. 5), generally comprising~~In general, samples taken close to the

boundary between the mylonites and unsheared rocks of the Fregon Subdomain (typically the uppermost few tens to one hundred metres~~).~~) were investigated. For the majority of samples, the assignment was straightforward since the inferred hanging wall samples are extremely low in thorium (<3 ppm), whereas most inferred footwall samples have values >8 ppm. Exceptions are samples SW14-243 and SW13-159, which have intermediate concentrations of 8 ppm and 6 ppm~~ and 8 ppm~~, respectively. Both samples were assigned to the footwall since subsequent samples further towards the hanging wall, respectively SW14-244 and SW13-161, could clearly still be attributed to the footwall. Alternatively, samples SW14-243 and SW13-159 could reflect imbrication of the Mulga Park and Fregon Subdomains, but this is not supported by any field observation.

In group (2), ~~four different transects were investigated (locations 2–4 and 6 in Fig. 5). Thorium~~thorium concentrations vary between 11 and 49 ppm (Table 2) but do not allow a clear distinction between samples derived from the footwall and hanging wall in a manner similar to the central and southern locations. This result is in accord with the airborne thorium concentrations, which also do not indicate a significant jump across the Woodroffe Thrust in these more northerly locations (Fig. 5).

central and southern studied locations

hanging wall of the Woodroffe Thrust

location (Fig. 1)	sample	lithology	coordinates (WGS 1984) longitude	coordinates (WGS 1984) latitude	data source	Th (ppm)	
9	SW14-029A	granite	131,74496	-26,00093	1	6	correlation based on geographical location
9	SW14-025	granite	131,73269	-26,01569	1	3	
9	SW14-030B	granite	131,74295	-26,00222	1	5	
17	FW13-173	granite	131,54138	-26,34104	1	3	
18	FW13-228	granite	131,56005	-26,37413	1	28	
-	MP-2	granite	131,74845	-25,99871	3	10	
-	MP94/500	granite	131,73549	-25,99535	3	4	
-	MP94/501	granite	131,74105	-25,99389	3	11	
-	W-12	granite	131,55670	-26,38583	2	19	
-	W-34d	granite	131,52310	-26,34528	2	6	
-	W-70	granite	131,63910	-26,40186	2	4	
-	W-96	granite	131,69440	-26,38511	2	8	
-	W-104	granite	131,70010	-26,38119	2	4	
-	W-127	granite	131,90190	-26,43750	2	7	
-	W-146	granite	131,87670	-26,35469	2	6	
-	W-148	granite	131,88030	-26,34653	2	10	
-	W-199a	granite	131,77080	-26,47550	2	54	
-	W-199b	granite	131,77080	-26,47550	2	63	
-	E-37	charnockite	132,27078	-26,19010	2	6	
-	E-38	charnockite	132,26899	-26,18286	2	3	
-	E-39	charnockite	132,14968	-26,22028	2	2	
-	W-32	charnockite	131,46100	-26,29419	2	26	
-	W-129	charnockite	131,89100	-26,38531	2	8	
16	NW13-043	felsic gneiss	131,49727	-26,28058	1	4	
16	SW13-032	felsic gneiss	131,49771	-26,28135	1	2	
19	NW13-016B	felsic gneiss	131,71053	-26,38530	1	28	
20	NW13-026	felsic gneiss	131,66087	-26,41038	1	20	
20	NW13-030	felsic gneiss	131,66258	-26,40675	1	1	
-	E-27	felsic gneiss	132,14091	-26,18857	2	3	
-	E-47	felsic gneiss	132,04583	-26,29111	2	2	
-	MP97/513	felsic gneiss	131,66461	-25,97300	3	12	
-	W-16dg	felsic gneiss	131,52810	-26,26806	2	6	
-	W-16ug	felsic gneiss	131,52810	-26,26806	2	8	
-	W-18	felsic gneiss	131,53810	-26,27472	2	21	
-	W-122adg	felsic gneiss	131,69830	-26,28992	2	3	
-	W-122aug	felsic gneiss	131,69830	-26,28992	2	8	
-	W-140b	felsic gneiss	131,84610	-26,43642	2	5	
-	W-142a	felsic gneiss	131,84050	-26,44422	2	N/D	
8	SW13-191	felsic gneiss	131,66264	-25,99911	1	N/D < 2	corr. based on Th conc.
11	SW14-181A	felsic gneiss	131,92595	-26,17664	1	N/D < 2	
11	SW14-182	felsic gneiss	131,92564	-26,17681	1	1	
12	NW13-187B	felsic gneiss	131,87917	-26,21151	1	1	
12	SW13-135A	felsic gneiss	131,87939	-26,21188	1	2	
12	SW13-135B	felsic gneiss	131,87939	-26,21188	1	2	
12	NW13-189	felsic gneiss	131,87935	-26,21191	1	2	
13	SW14-246A	felsic gneiss	131,84444	-26,25262	1	2	
14	SW13-164	felsic gneiss	131,77463	-26,30772	1	3	

footwall of the Woodroffe Thrust

location (Fig. 1)	sample	lithology	coordinates (WGS 1984) longitude	coordinates (WGS 1984) latitude	data source	Th (ppm)	
12	SW13-122A	granite	131,87206	-26,20364	1	73	correlation based on geographical location
12	SW13-123	granite	131,87229	-26,20379	1	7	
12	NW13-184	granite	131,87823	-26,20914	1	16	
12	NW13-185B	granite	131,87830	-26,20946	1	14	
14	SW13-151	granite	131,77438	-26,30117	1	20	
14	SW13-153	granite	131,77411	-26,30173	1	N/D < 2	
-	MP94/502	granite	131,78418	-25,95562	3	55	
-	MP94/503	granite	131,62926	-25,86096	3	30	
-	BJ96/178	granite	131,48641	-25,78867	3*	18	
-	BJ96/201	granite	131,39771	-25,79945	3*	195	
-	BJ96/276	granite	131,44734	-25,97263	3*	18	
-	MP96/505	granite	131,64751	-25,95006	3*	35	
-	MP96/509	granite	131,64996	-25,94452	3	12	
12	SW13-125	felsic gneiss	131,87338	-26,20470	1	27	
-	MP97/43	felsic gneiss	131,81710	-25,98836	3	10	
8	GW13-415	felsic gneiss	131,66256	-25,99928	1	15	corr. based on Th conc.
8	SW13-193	felsic gneiss	131,66256	-25,99928	1	16	
8	SW13-192	felsic gneiss	131,66258	-25,99915	1	23	
11	SW14-179	felsic gneiss	131,92603	-26,17661	1	15	
12	SW13-134	felsic gneiss	131,87913	-26,21151	1	9	
13	SW14-243	felsic gneiss	131,83942	-26,25476	1	8	
13	SW14-244	felsic gneiss	131,83949	-26,25472	1	13	
14	SW13-159	felsic gneiss	131,77375	-26,30666	1	6	
14	SW13-161	felsic gneiss	131,77445	-26,30759	1	14	

data source:

1	this study
2	Camacho (1997)
3	Young et al. (2002)
*	values erroneously published in Young et al. (2002), but correctly presented here (personal communication A. Camacho)
N/D	below detection limit

northern studied locations

location (Fig. 1)	sample	lithology	coordinates (WGS 1984) longitude	coordinates (WGS 1984) latitude	data source	Th (ppm)
6	SW13-321	granite	132,14333	-25,99178	1	23
6	SW13-322	granite	132,14340	-25,99191	1	49
3	NW13-134A	felsic gneiss	131,45284	-25,85477	1	34
2	SW13-173A	felsic gneiss	131,45334	-25,84543	1	17
2	SW13-173C	felsic gneiss	131,45334	-25,84543	1	31
3	FW13-093	felsic gneiss	131,45213	-25,85455	1	11
4	SW14-006	felsic gneiss	131,45047	-25,87174	1	20
6	SW13-323A	felsic gneiss	132,14344	-25,99211	1	19
6	SW14-034A	felsic gneiss	132,14337	-25,99224	1	12

Table 2: Thorium concentrations in felsic gneisses and granitoids from the hanging wall and footwall of the Woodroffe Thrust, central Musgrave Block.

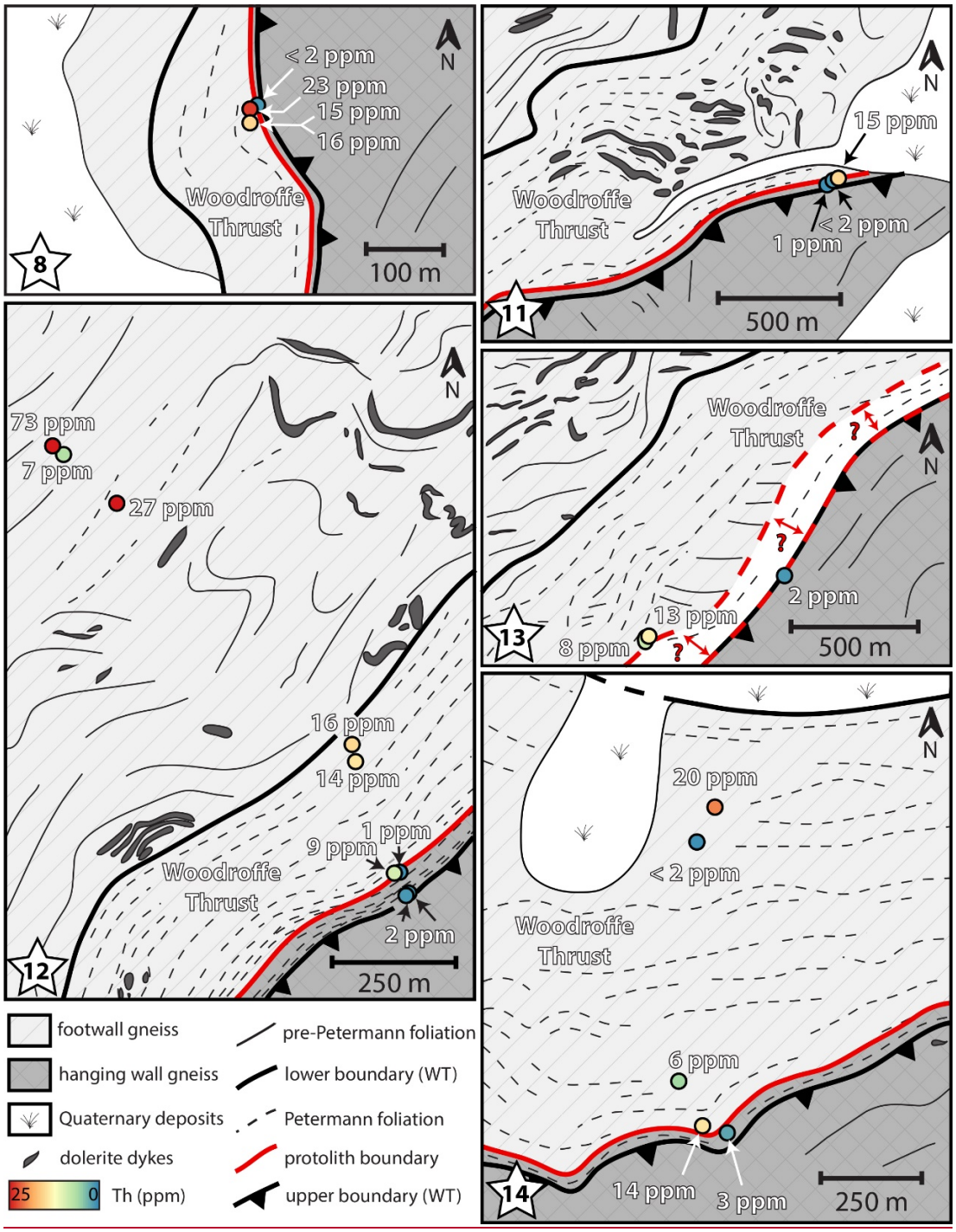

Figure 6: Sample-specific thorium (Th) concentrations (measured by γ-ray spectrometry) plotted across the Woodroffe Thrust (WT) mylonites at locations 8 and 11-14 (Fig. 1). The original boundary between the lower-thorium hanging wall and higher-thorium footwall is inferred (red line).

5.2 Determination of the hanging wall-footwall boundary

Measured thorium concentrations indicate that in locations 8 and 11-14 (Fig. 5) the uppermost mylonites of the Woodroffe Thrust developed in the lower-thorium Fregon Subdomain (Table 2). These results are in agreement with the proposed identification of hanging wall reworking based on field appearance. Similar field relationships, such as progressive downwards mylonitization of units clearly forming part of the hanging wall ~~pseudotachylyte breccia~~, also ~~indicates~~indicate limited reworking of the Fregon Subdomain at locations 4 and 6 (Fig. 5). However, the lack of a clear contrast in thorium concentrations between footwall and hanging wall in ~~the northern~~these locations precludes any verification of these field observations, as well as any independent determination of the thickness of hanging wall-derived mylonites in the thrust zone. We therefore excluded these northern transects when using thorium concentration as a proxy to map the original boundary between the hanging wall and footwall (Fig. 6). It was also not possible to precisely determine the boundary at location 13 (Fig. 1), due to a large lateral gap between the last sample assigned to the footwall and the first sample assigned to the hanging wall. In an attempt to quantitatively calculate the degree of hanging wall/footwall reworking into the total mylonite zone, we applied trigonometry based on the geometrical arrangement sketched in Fig. 4a. The only modification was that the lower mylonite boundary was now defined by the newly reconstructed boundary between hanging wall and footwall. Results are summarized in Table 3. In contrast to the 250 m proposed by Bell (1978) for the Amata area (western edge of Fig. 1), our results indicate that only the lowermost 3 m of the Fregon Subdomain were reworked into the Woodroffe Thrust mylonites at location 8, increasing up to 18-40 m at locations 11-14 (Fig. 1). These values represent 3-6 % of the entire thickness of the Woodroffe Thrust mylonites (Table 1) at locations 8, 11 and 14 and up to 13 % at location 12 (Fig. 1). However, the difference in elevation (p) is not well defined over short distances (q) given the limited (30x30 m) resolution of the digital elevation model (ASTER). This can introduce a significant uncertainty into the calculation of the degree of hanging wall reworking. Nevertheless, our analysis clearly shows that the majority of mylonites developed in the Mulga Park Subdomain (footwall) rather than the Fregon Subdomain (hanging wall).

location	coordinates (WGS 1984)		trigonometrical parameters			
(Fig. 1)	longitude	latitude	α (°)	p (m)	q (m)	T (m)
8	132.143	-25.992	10	1	10	3
11	131.926	-26.177	28	5	30	18
12	131.879	-26.212	21	22	55	40
13	131.844	-26.253	-	-	-	>0
14	131.774	-26.308	22	9	30	20

Table 3: Angle of dip (α), elevation difference (p), apparent thickness (q) and true thickness (T) of the Woodroffe Thrust mylonites derived from the hanging wall.

6 Presence or absence of fluids during mylonitization

The syn-deformational presence or absence of fluids in the study area is established from a series of field and thin section observations. These include the regional variation in: (1) syntectonic quartz veins, (2) introduction of carbon and (3) plagioclase stability and breakdown.

6.1 Quartz veins

Syntectonic quartz veins (Fig. 7a) and associated quartz-rich pegmatite dykes are uncommon throughout the field area, being generally absent in the southern locations ~~10-15~~ and only locally present in the northern locations ~~1-9~~ (Fig. 8a). These quartz veins crosscut the mylonitic fabric but were themselves variably deformed during subsequent shearing, providing direct field evidence that they were broadly coeval with the Woodroffe Thrust, and thus associated with the Petermann Orogeny. Sense of shear is both top-to-north and top-to-south, which is contrary to the dominant top-to-north shear sense associated with the Woodroffe Thrust, but has also been documented by Bell and Johnson (1992) in the Amata region (western edge of Fig. 1). Quartz veins are boudinaged within the mylonitic foliation and, although deformed, did not preferentially localize strain (Figs. 7a,b).

6.2 Introduction of carbon

Finely dispersed calcite is locally found with very low modal abundance (typically <1 %) in the otherwise non-carbonaceous rocks of the central Musgrave Block (Fig. 7c). Calcite-bearing samples are present throughout the study area, but are generally more common ~~towards~~in the north (Fig. 8b). Microstructures indicate that the fine-grained (<10 µm) calcite nucleated during shearing (Fig. 7c). Calcium was made available from dynamic "recrystallization" of plagioclase to new grains with lower anorthite content (Wex et al., 2017), but carbon ~~requires~~cannot have an ~~external fluid since~~immediately local source, because the ~~protoliths are~~studied rocks were initially entirely non-carbonaceous. In the attempt to ~~establish~~place further constraints on the origin of this fluid, carbon and oxygen isotopes of calcite were measured (Supporting Information S2), yielding mean average values of -4.1 ‰ for $\delta^{13}C_{Cal}$ (V-PDB) and +10.1 ‰ for $\delta^{18}O_{Cal}$ (SMOW). Within the same samples, the whole rock isotopic signature $\delta^{13}C_{whole\ rock}$ (V-PDB) is always lower (on average by 2.7 ‰) than the corresponding $\delta^{13}C_{Cal}$ values.

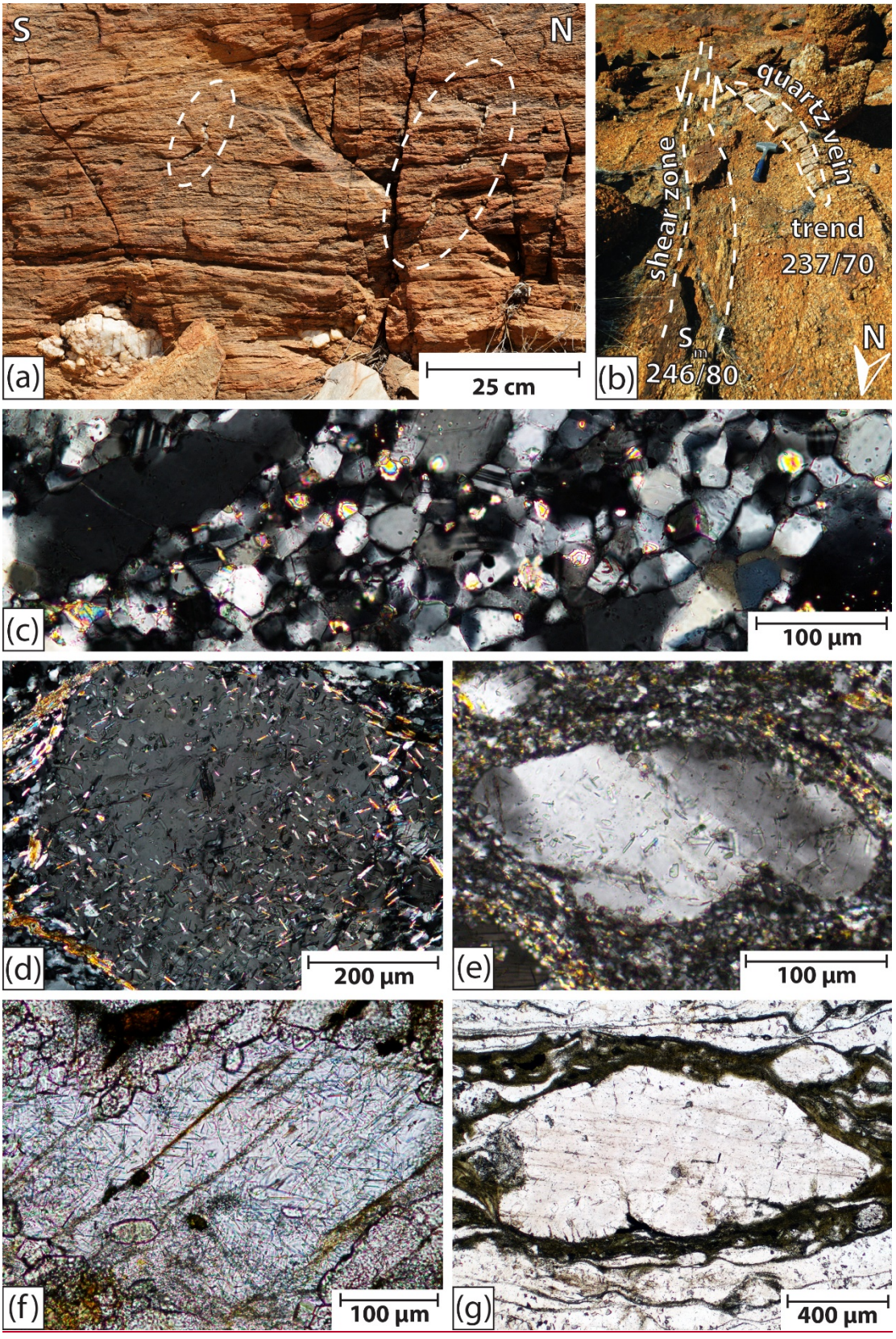
S
N
(a)
25 cm
quartz vein
shear zone
trend
237/70
S_m
246/80
N
(b)
(c)
100 µm
(d)
200 µm
(e)
100 µm
(f)
100 µm
(g)
400 µm

Figure 7: Field and thin section images providing evidence for the presence or absence of ~~aqueous~~ fluids during deformation. (a) ~~Syntectonically developed quartz~~Quartz veins (encircled) crosscut the mylonitic foliation of the Woodroffe Thrust ~~but were subsequently sheared and rotated,~~showing a sigmoidal shape consistent with rotation during overall top-to-north shearing. The quartz vein at the bottom of the picture is boudinaged and did not localize deformation. Outcrop NW15-264 (coordinates: 131.46883, -25.83040; location 1 in Fig. 1). (b) Quartz vein adjacent to a sinistral shear zone that is not reactivated, even though shear zone and quartz vein are almost parallel to each other. Abbreviation: S_m = mylonitic foliation. Outcrop SW13-200 (coordinates: 131.73810, -25.99564; location 9 in Fig. 1). (c) Finely dispersed calcite (high birefringence) between recrystallized feldspar grains under crossed-polarized light. Thin section is not oriented. Sample NW14-423A (coordinates: 131.84368, -26.11423; location 10 in Fig. 1). (d) Plagioclase clast with muscovite (higher birefringence) and epidote (lower birefringence) inclusions under crossed-polarized light. Thin section is oriented N-S (left-right). Sample SW14-214A (coordinates: 131.44416, -25.90284; location 5 in Fig. 1). (e) Plagioclase clast with epidote inclusions under crossed-polarized light. Thin section is oriented N-S (left-right). Sample GW13-415 (coordinates: 131.66256, -25.99928; location 8 in Fig. 1). (f) Plagioclase clast with kyanite inclusions (greenish needles) and neo-crystallized garnet under plane-polarized light. Thin section is not oriented. Sample SW13-167 (coordinates: 131.77475, -26.30845; location 14 in Fig. 1). (g) Inclusion-free plagioclase clast under plane-polarized light. Thin section is oriented NNE-SSW (left-right). Sample SW13-318 (coordinates: 132.14311, -25.99142; location 6 in Fig. 1).

6.3 Plagioclase stability and breakdown

~~Plagioclase recrystallized in the Woodroffe Thrust mylonites and associated shear zones (Bell and Johnson, 1989; Wex et al., 2017) forming typical "core and mantle structures". Mineral inclusions within plagioclase clasts are common and allow the distinction of four different types of clasts, respectively termed microstructures 1 to 4:~~

~~Plagioclase studded with abundant inclusions of epidote and muscovite (Fig. 7d). This type is, with one exception, restricted to the northern locations 1-9 (Fig.~~Plagioclase dynamically recrystallized in the Woodroffe Thrust mylonites and associated shear zones (Bell and Johnson, 1989), forming typical "core-and-mantle structures". The composition of the newly recrystallized grains ranges from albite/oligoclase in felsic rocks to oligoclase/andesine in mafic rocks (Wex et al., 2017). Mineral inclusions within plagioclase clasts are common and allow the distinction of four different types of clasts, respectively termed microstructures 1 to 4:

(1) Plagioclase studded with abundant inclusions of epidote and muscovite (Fig. 7d). This type is, with one exception, restricted to the northern locations (Fig. 8c).
(2) Plagioclase containing only epidote inclusions (Fig. 7e), with a modal abundance far lower than that of epidote + muscovite inclusions of microstructure 1. This microstructure is restricted to the central locations ~~8-13~~ (Fig. 8c).
(3) Plagioclase crowded with kyanite needle inclusions (Fig. 7f) (see Supporting Information B of Wex et al. (2017) for identification techniques). This microstructure is restricted to the southernmost locations ~~13-15~~ (Fig. 8c).
(4) Plagioclase free of inclusions (Fig. 7g). This microstructure is found in ~~the~~almost all locations ~~4-13~~ (Fig. 8c).

Figure 8c shows that the type of inclusions in plagioclase varies in a N-S direction, i.e. parallel to the tectonic transport direction of the Woodroffe Thrust. From north to south, inclusions progressively change from muscovite + epidote (microstructure 1), to epidote (microstructure 2), and to kyanite (microstructure 3), with inclusion-free plagioclase clasts (microstructure 4) occurring throughout. There is no apparent variation of the type of plagioclase inclusions along strike of the Woodroffe Thrust (i.e. E-W).

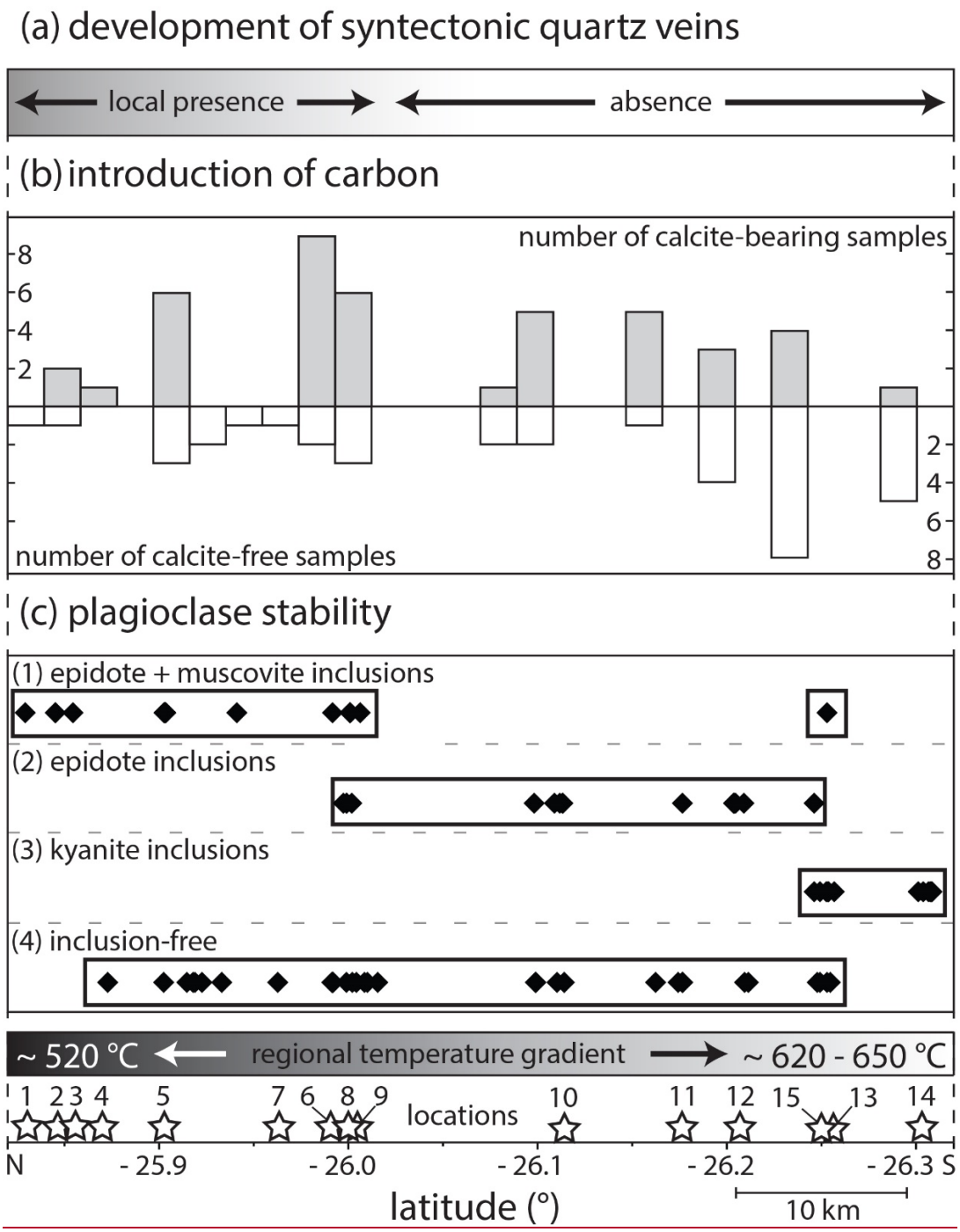

Figure 8: Regional variation in the development of (a) syntectonic quartz veins, (b) the introduction of carbon and (c) plagioclase stability and breakdown, each plotted against sample latitude. The regional temperature gradient (Wex et al., 2017) and the position of the studied locations (Fig. 1) are indicated.

7 Abundance of hydrous minerals

~~The modal abundance of hydrous minerals in deformed and undeformed pseudotachylytes (representative compilation in Supporting Information S3) from felsic footwall and hanging wall samples was determined by image analysis of backscattered electron (BSE) images (method outlined in the Supporting Information S1). The different amounts of hydrous minerals between the pseudotachylytes should reflect compositional variations between the host rocks from which they formed. The results, summarized in Table 4, indicate that matrix mineral assemblages of felsic pseudotachylytes from the hanging wall and footwall are similar to each other. These assemblages dominantly comprise Pl + Kfs + Qz + Bt + Mag + Ilm with individual samples also containing Ep, Grt, Cpx, Opx, Ky, Ms, Rt or Hbl. However, there is a strong contrast with regard to the modal abundance of hydrous minerals. Samples have been sorted into northern (locations 1–5 in Fig. 1), central (locations 6–9 in Fig. 1) and southern location groups (locations 11–14 in Fig. 1), revealing that: (i) the abundance of hydrous minerals decreases from north to south in both the hanging wall and the footwall; and (ii) at similar latitude, the footwall rocks are more hydrous than the hanging wall rocks. Two samples (SW14-029A and SW14-179) do not fit this regional trend and these outliers have been excluded in calculating the mean values, as they mask what are otherwise apparent trends.~~

Pseudotachylytes have been identified as preferred discontinuities for nucleation of ductile shear zones and strain localization under mid- to lower crustal conditions (Andersen and Austrheim, 2006; Austrheim and Andersen, 2004; Hawemann et al., 2014; Lund and Austrheim, 2003; Menegon et al., 2017; Passchier, 1982; Pennacchioni and Cesare, 1997; Pittarello et al., 2012; Wex et al., 2014, 2017). In order to study the control of host rock mineralogy on shear initiation, the modal abundance of hydrous minerals in deformed and undeformed pseudotachylytes (representative compilation in Supporting Information S3) from felsic footwall and hanging wall samples was determined by image analysis of backscattered electron (BSE) images (method outlined in the Supporting Information S1). The different amounts of hydrous minerals between the pseudotachylytes should reflect compositional variations between the host rocks from which they formed. The results, summarized in Table 4, indicate that matrix mineral assemblages of felsic pseudotachylytes from the hanging wall and footwall are similar to each other. These assemblages dominantly comprise Pl + Kfs + Qz + Bt + Mag + Ilm with individual samples also containing Ep, Grt, Cpx, Opx, Ky, Ms, Rt or Hbl. However, there is a strong contrast with regard to the modal abundance of hydrous minerals in the studied pseudotachylytes. Samples have been grouped according to their latitude coordinates, revealing that: (i) the abundance of hydrous minerals decreases from north to south in both the hanging wall and the footwall; and (ii) at similar latitude, the footwall rocks are more hydrous than the hanging wall rocks. Two samples (SW14-029A and SW14-179) do not fit this regional trend and these outliers have been excluded in calculating the mean values, as they mask what are otherwise clear trends.

hanging wall of the Woodroffe Thrust									footwall of the Woodroffe Thrust								
	location (Fig. 1)	sample	pristine	sheared	BSE images	coordinates (WGS 1984)	mineral assemblage (pseudotachylyte)	hydrous minerals (%)		location (Fig. 1)	sample	pristine	sheared	BSE images	coordinates (WGS 1984)	mineral assemblage (pseudotachylyte)	hydrous minerals (%)
north	2	SW13-174A	x		3	131.45304 -25.84532	Pl + Kfs + Bt + Cpx + Qz + Mag + Ilm	10		2	SW13-171	x		3	131.45397 -25.84535	Qz + Bt + Ms + Ep + Mag + Pl ± Kfs	40
	3	NW13-139	x		3	131.44826 -25.85366	Kfs + Pl + Mag + Bt	4	av. 10 %	2	SW13-171		x	3	131.45397 -25.84535	Qz + Bt + Ms + Ep + Mag + Pl ± Kfs	40
	3	FW13-096	x		2	131.45034 -25.85414	Pl + Kfs + Bt + Hbl + Ep + Mag	7		3	NW13-134A		x	2	131.45284 -25.85477	Pl + Qz + Kfs + Ep + Bt	20	av. 30 %
	3	SW13-102	x		4	131.45164 -25.85433	Pl + Bt + Opx + Qz + Mag	17		3	FW13-093		x	3	131.45213 -25.85455	Pl + Qz + Kfs + Hbl + Bt + Mag + Ilm	29	
										5	SW14-228A	x		3	131.44158 -25.90365	Pl + Kfs + Ep + Bt + Mag ± Ilm	20	
central	8	SW13-191	x		4	131.66264 -25.99911	Pl + Cpx + Bt + Qz + Opx + Mag	16		6	SW13-321		x	5	132.14333 -25.99178	Pl + Kfs + Qz + Bt + Ep + Grt + Mag + Ilm	13	
	9	SW14-029B		x	3	131.74496 -26.00093	Pl + Kfs + Bt + Qz + Grt + Ep + Mag	13		6	SW13-323A	x		4	132.14344 -25.99211	Pl + Kfs + Bt + Qz + Mag + Ilm	10	
	9	SW14-029A	x		3	131.74496 -26.00093	Hbl + Pl + Kfs + Qz + Bt + Ilm	33*	av. 8 % [12 %]	6	SW13-323A	x		3	132.14344 -25.99211	Pl + Kfs + Bt + Qz + Mag + Ilm	10	av. 10 %
	9	SW14-029A	x		2	131.74496 -26.00093	Kfs + Pl + Qz + Bt + Mag	3		6	SW13-323A	x		3	132.14344 -25.99211	Pl + Kfs + Bt + Qz + Mag + Ilm	8	
	9	SW14-025		x	6	131.73269 -26.01569	Pl + Kfs + Opx + Qz + Bt + Mag + Ilm + Cal	2		8	SW13-192		x	2	131.66258 -25.99915	Kfs + Pl + Qz + Bt + Ep + Hbl + Grt + Mag	8	
	9	NW13-203	x		3	131.74318 -26.00442	Kfs + Pl + Grt + Bt + Qz + Mag	5										
south	11	SW14-181A	x		5	131.92595 -26.17664	Kfs + Pl + Qz + Cpx + Grt + Mag + Bt	1		11	SW14-179		x	3	131.92603 -26.17661	Pl + Qz + Kfs + Hbl + Grt + Opx + Ilm + Mag ± Bt	21*	
	11	SW14-181B	x		-	131.92595 -26.17664	Pl + Kfs + Qz + Cpx + Grt + Ilm ± Bt	<1	av. 1 %	12	SW13-134		x	2	131.87913 -26.21151	Pl + Kfs + Qz + Bt + Opx + Grt + Ilm	3	
	11	SW14-181B	x		2	131.92595 -26.17664	Pl + Kfs + Grt + Qz + Cpx + Bt + Ilm	3		13	SW14-237C	x		4	131.83544 -26.25303	Kfs + Pl + Bt + Mag	5	av. 4 % [7 %]
	11	SW14-181B	x		-	131.92595 -26.17664	Pl + Kfs + Grt + Opx + Cpx + Qz + Ilm ± Bt	<1		13	SW14-244		x	2	131.83949 -26.25472	Pl + Kfs + Qz + Bt + Hbl + Ilm + Grt	7	
										14	SW13-159		x	-	131.77375 -26.30666	Pl + Kfs + Cpx + Grt + Qz + Ky + Ilm + Rt	0	

Table 4: Modal abundance of hydrous minerals in felsic pseudotachylytes from the hanging wall and footwall of the Woodroffe Thrust, central Musgrave Block[a].

[a] Extreme outliers (*) are not considered. Mineral assemblages are listed in order of decreasing modal abundance (from left to right) with hydrous minerals underlined. A representative compilation of pseudotachylytes is given in the Supporting Information S3.

Figure 9 deleted

8 Discussion

8.1 Plagioclase breakdown reactions

Within the range of ~~miderustal~~mid- to lower crustal conditions, as estimated for the Woodroffe Thrust (Wex et al., 2017), the following plagioclase breakdown reactions are relevant ~~(Fig. 9):~~:

(1) An + Or + H_2O = Ms + Ep + Qz (Kretz, 1963; Ramberg, 1949)
(2) An + Grs + H_2O = Ep + Qz (Kretz, 1963)
(3) An = Grs + Ky + Qz (Boyd and England, 1961; Hariya and Kennedy, 1968)
(4) An + H_2O = Ep + Ky + Qz (Goldsmith, 1982; Kretz, 1963; Ramberg, 1949)

For the sake of simplicity, ~~none of these reactions~~these reactions proposed in the cited publications are restricted to the system Ca-K-Al-Si-OH, and in particular do not consider the presence of iron. However, iron is certainly necessary to account for the crystallization of epidote and was potentially derived from relict iron-bearing minerals (e.g., magnetite ~~or~~, ilmenite, biotite or garnet). Microstructure 1 is unequivocally correlated with hydration reaction 1. Reaction 2 is capable of producing microstructure 2, but garnet has been interpreted to serve as a calcium-sink rather than source during the high-pressure Petermann Orogeny (Camacho et al., 2009). Alternatively, we propose that the decrease in anorthite content during plagioclase recrystallization (Wex et al., 2017) provided the necessary source of calcium for producing microstructure 2. Microstructure 3 is correlated with reaction 3. Reactions 3 and 4 represent the high-pressure breakdown of plagioclase under anhydrous and hydrous conditions, respectively. According to Wayte et al. (1989), the transition between the two competing reactions occurs at a water activity of ca. 0.004 for pressure and temperature conditions similar to those in the more southerly footwall locations. In samples with microstructure 3, epidote is never observed as a secondary inclusion phase together with kyanite (Supporting Information S4), indicating that reaction 3 ~~was~~ always ~~preferred~~prevailed over reaction 4.

8.2 Fluid activity

In the southern locations ~~13–15~~ (Fig. 1), plagioclase breakdown by reaction 3 indicates that water was not sufficiently available to drive reaction 4 (Goldsmith, 1980, 1982; Wayte et al., 1989). Consequently, reaction 3 is a good indicator for very low water activities (<0.004; Wayte et al., 1989) and the absence of a free ~~aqueous~~ fluid phase during deformation, since only very small amounts of water (ca. 20 ppm) are required for mineral reactions in a solid silicate system (Milke et al., 2013). Similarly, relict plagioclase clasts without any inclusions (microstructure 4) also indicate the absence of a free ~~aqueous fluids~~fluid phase, as the studied rocks were all metastable with respect to hydration reactions 1, 2 and 4 ~~(Fig. 9).~~. Consequently, any of these

breakdown reactions would have rapidly consumed any available free fluid, since all other reactants were present in the studied samples. Vice versa, plagioclase breakdown by reaction 1 clearly indicates the presence of a free ~~aqueous~~fluid phase during deformation. Reaction 2 also involves hydration, as indicated by the marginal presence of epidote in plagioclase clasts (microstructure 2). However, free ~~aqueous~~ fluids were not sufficiently available to facilitate reaction 1. Hence, we ~~favor~~favour the interpretation that microstructure 2 indicates largely anhydrous conditions, with only very minor fluid introduction.

Based on the classification above, the regional availability of a free ~~aqueous~~ fluid phase during deformation, respectively termed "wet" and "dry", can be determined from the mineral inclusions in plagioclase (Fig. 8c) and the corresponding inferred breakdown reactions (Sect. 8.1). The distinction is purely qualitative and refers only to whether or not free ~~aqueous~~ fluid was sufficiently available to facilitate the hydrous breakdown reaction 1. Consequently, the studied field area is characterized as dominantly "dry" (microstructures 2, 3 and 4) with a progression towards locally "wet" conditions (microstructure 1) in most of the northernmost exposures (Fig. ~~10~~9). The regional variation in (1) the development of syntectonic quartz veins (Fig. 8a) and (2) the introduction of carbon (Fig. 8b) are each consistent with this interpretation (Fig. ~~10~~9). However, within a single location, individual samples can have a "wet" microstructure 1 while others still preserve a "dry" microstructure 4 (Fig. 8c), indicating that the fluids were only present on a very local scale. ~~This is additionally supported by the coeval development of a hydrous (Pl + Opx + Grt + Hbl + Ilm + Mag ± Cpx ± Bt) and an anhydrous mineral assemblage (Pl + Opx + Grt + Cpx + Kfs + Qz + Ilm + Mag) within a single thin section of a sheared dolerite dyke from the footwall of the Woodroffe Thrust (Supporting Information S5).~~Generally "dry" conditions are also in agreement with the fact that the metamorphic overprint during the Petermann Orogeny occurred under lower grade conditions compared to the earlier Musgravian Orogeny, and thus facilitated water consumption rather than water release.

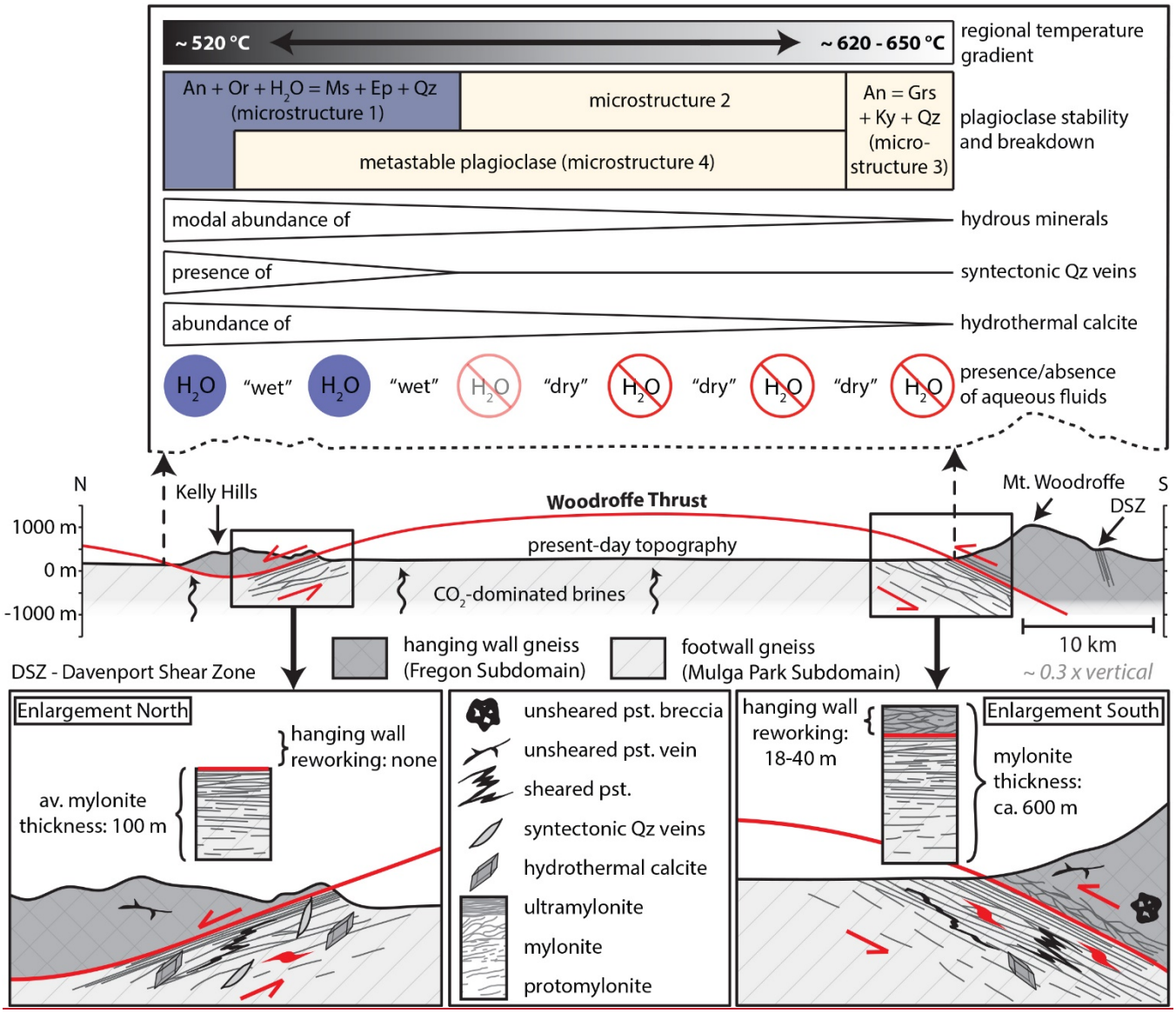

Figure ~~10~~9: Projected schematic cross section through the central Musgrave Block. The horizontal scale is compressed by a factor of 3.5 with respect to the vertical scale. The regional temperature gradient is taken from Wex et al. (2017).

8.3 Fluid source

Based on the above ~~quantification~~qualitative estimate of "fluid activity" in the study area, it is evident that aqueous ~~fluids~~ and CO_2-~~dominated brines~~ bearing fluids were introduced in the northern exposures of the Woodroffe Thrust (Fig. ~~10~~9). However, there does not seem to be any obvious link between the infiltration of the aqueous ~~fluids~~ and ~~that of~~ the CO_2-~~dominated~~

~~brines~~bearing fluids, since samples that preserve a "wet" microstructure 1 are not necessarily calcite-bearing and vice versa (Figs. 8b,c).

8.3.1 Aqueous fluids

Aqueous fluids infiltrating into the footwall of the Woodroffe Thrust were unlikely to have been derived from the "~~dry~~drier" hanging wall (Table 4) and consequently~~,~~ must originate from units within or underlying the current level of exposure of the footwall. Gneisses and granitoids in the "wet" northern part of the study area are clearly interleaved with and juxtaposed onto the basal units of the Amadeus Basin (Wells et al., 1970), as evident from outcrops of Dean Quartzite (Forman, 1965; Young et al., 2002) immediately west of the Kelly Hills klippe ~~(locations 1-5 in Fig. 1).~~ These Neoproterozoic sedimentary rocks represent an ideal source for aqueous fluids since they were metamorphosed and dehydrated during the Petermann Orogeny (Wells et al., 1970). However, based on regional-scale geometric reconstructions, it has been argued that the Woodroffe Thrust and potentially underlying thrust planes developed in-sequence (Wex et al., 2017). If this is true, then the Dean Quartzite was only imbricated below the northernmost studied locations after movement and deformation on the Woodroffe Thrust had largely ceased and the dynamic microstructures had already been frozen in. Therefore, we prefer a model in which the aqueous fluids were released from the granitoids and upper amphibolite facies gneisses within the footwall. Such a model is in agreement with the fact that the regional trend towards higher abundance of hydrous minerals in the north parallels the shift towards "wet" conditions, as indicated by the plagioclase breakdown reactions (Fig. ~~10~~9). An internal source is also consistent with the conclusion that "wet" conditions were only present on a very local scale and that "wet" and "dry" samples are often preserved in close proximity. Consequently, we consider that the studied field area was not infiltrated by externally derived aqueous fluids and remained a relatively closed system.

8.3.2 CO_2-~~dominated brines~~bearing fluids

The fact that the gneisses and granitoids of the central Musgrave Block are entirely non-carbonaceous (Collerson et al., 1972; Major, 1973; Major and Conor, 1993; Scrimgeour and Close, 1999) argues for an external source of the CO_2-~~dominated brines.~~bearing fluids. Carbon and oxygen isotropic signatures were measured in order to provide constraints on its nature. The results for $\delta^{18}O$ are in agreement with calcite crystallization temperatures of 500-600 °C, while $\delta^{13}C$ values are strongly rock-buffered~~, but potentially indicate a mantle origin (~~ (see Supporting Information S2 for more details).

8.4 Distribution of ductile deformation

The distribution of thorium establishes that the Woodroffe Thrust mylonites preferentially developed in the Mulga Park rather than the Fregon Subdomain (Fig. 6). This conclusion is in agreement with our field observations and with those of Bell and Etheridge (1976), Camacho et al. (1995) and Flottmann et al. (2004). However, it is evident from our results that in the southern locations ~~(11-14 in Fig. 1)~~ the lowermost hanging wall was also involved in the mylonitization process (Table 3). We discuss below the potential processes guiding the large-scale distribution of ductile deformation in the Woodroffe Thrust.

8.4.1 Footwall/hanging wall reworking

The proportion of the total shear strain accommodated in the narrow mylonitic to ultramylonitic zones developed in the lowermost hanging wall and uppermost footwall cannot be determined. However, what could be determined in this study is the relative thickness of the mylonite zones, using thorium concentrations to distinguish the original hanging wall and footwall protoliths. From this it is established that the hanging wall-derived parts of the Woodroffe Thrust generally make up <10% of the entire width of the mylonitic zone. This preferential development of a broader mylonite zone in the Mulga Park Subdomain footwall rather than in the Fregon Subdomain hanging wall is contrary to the expected simple model of a thrust or reverse fault system ~~(e.g., Manecktelow, 1985, his Fig. 11).~~(e.g., Mancktelow, 1985; Passchier, 1984). Such a model would predict an asymmetric strain profile where the mylonite zone occurs in the initially "hotter" hanging wall rather than the "colder" footwall. An inverse distribution of ductile deformation, as a consequence of asymmetric thermal weakening, would be in agreement with the flower-like structure model proposed by Camacho and McDougall (2000) for the central Musgrave Block. Based on the preservation of pre-Petermann K-Ar, ^{40}Ar~~/~~-^{39}Ar and Rb-Sr ages in hornblende, muscovite, biotite and K-feldspar in the undeformed gneissic country rocks, Camacho and McDougall (2000) argued that the Fregon Subdomain was rapidly buried and exhumed in less than 40 Myr. Consequently, these rocks failed to thermally equilibrate to temperatures above 350 °C at a pressure of ~1.2 GPa. With this tectonic model, the hanging wall should have been at temperatures <350 °C (Camacho and McDougall, 2000) and thus should have been colder than the footwall (>500 °C; Wex et al., 2017). In such a model, thermal weakening could indeed account for preferential mylonitization of the Mulga Park Subdomain. However, Wex et al. (2017) and Hawemann et al. (2017) demonstrated that Petermann Orogeny metamorphic assemblages throughout the study area are directly comparable in dynamically and statically recrystallized units, arguing that the estimated metamorphic conditions were ambient and differed little between shear zones and country rock. In addition, Wex et al. (2017) found that the syntectonic metamorphic conditions are similar in the hanging wall and footwall at the same locality, arguing against thermal weakening as a cause of the preferential mylonitization of the Mulga Park Subdomain (Camacho and McDougall, 2000).

Pseudotachylytes have been identified as preferred nucleation discontinuities for shearing under mid- to lower crustal conditions (Andersen and Austrheim, 2006; Austrheim and Andersen, 2004; Hawemann et al., 2014; Lund and Austrheim, 2003; Menegon et al., 2017; Passchier, 1982; Pennacchioni and Cesare, 1997; Pittarello et al., 2012; Wex et al., 2014, 2017). In the Musgrave Block however, the presence of precursor pseudotachylyte cannot account for the observed inverse distribution of ductile deformation, as they are significantly more abundant in the hanging wall compared to the footwall (Camacho et al., 1995; Lin et al., 2005).

A potential explanation for the observed inverse gradient of ductile deformation along the Woodroffe Thrust is a rheological contrast between hanging wall and footwall assemblages, resulting in different degrees, and potentially different processes, of water-assisted weakening in quartz and feldspar ~~(e.g., Griggs, 1967, 1974; Griggs and Blacic, 1965; Hobbs, 1985; Kronenberg et al., 1990; Stünitz et al., 2017; Tullis and Yund, 1989)~~(e.g., Fitz Gerald et al., 2006; Griggs, 1967, 1974; Griggs and Blacic,

1965; Hobbs, 1985; Kronenberg et al., 1990; Mancktelow and Pennacchioni, 2004; Stünitz et al., 2017; Tullis and Yund, 1989). As discussed in Sect. 8.3.1, the rocks in the study area represent a relatively closed system with respect to the presence or absence of aqueous fluids~~. Hence,~~, although some CO_2 introduction from an external source is necessary to account for the syntectonic growth of very minor amounts of calcite in previously non-carbonaceous rocks. The availability of aqueous fluids is thus directly linked to the abundance of hydrous minerals in these rocks, which is observed to decrease from north to south (Fig. ~~10~~9). Similarly, the contrasting abundance of hydrous minerals in hanging wall and footwall (Table 4) indicates that there is consistently a higher potential for generating aqueous fluids in the footwall than in the hanging wall. ~~Overall,~~If sufficient water was available, this could facilitate a preferential rheological weakening of the footwall due to new growth of micas and associated phyllonite development. However, this is not observed because the majority of the studied rocks are still relatively "dry", so that only slight differences in the abundance of water could facilitate an asymmetric ~~localization~~distribution of ductile deformation as a consequence of water-assisted weakening. The preferential mylonitization of the Mulga Park relative to the Fregon Subdomain (Fig. 6) therefore seems to be largely controlled by the precursor mineralogy established as the result of the earlier (ca. 1200 Ma) Musgravian Orogeny metamorphism, with peak conditions of upper amphibolite facies in the footwall but granulite facies in the hanging wall. This supports the initial hypothesis of Bell and Etheridge (1976) and Camacho et al. (1995) that a more hydrous footwall underlying an anhydrous hanging wall can facilitate an inverted gradient of ductile deformation.

These arguments may explain the overall preferential ~~localization~~distribution of deformation in the Mulga Park Subdomain, but fail to provide an adequate explanation for why the lowermost Fregon Subdomain was also incorporated into the mylonites (Figs. ~~2, 6, 10). The generally low abundance of hydrous minerals in both hanging wall and footwall in the "dry" southern locations (11–14 in Table 4) potentially promoted a similar rheological response in both units. Locally, there may be no contrast at all in protolith composition, which might explain the marginal mylonitization of the lowermost Fregon Subdomain. Reworking of the hanging wall may also~~2, 6, 9). This reworking of the hanging wall may potentially have been guided by the presence of pseudotachylytes, which are ubiquitous and voluminous in the immediate hanging wall of the Woodroffe Thrust (Camacho et al., 1995; Lin et al., 2005).

8.4.2 Variation in mylonite thickness

Mylonite thickness in the study area does not ~~appear to~~ significantly vary parallel to strike (i.e. E-W). However, from south to north, i.e. parallel to the direction of tectonic transport, the Woodroffe Thrust mylonitic zone gradually decreases in thickness from over 600 m to less than 100 m (Table 1~~), indicating~~). This potentially indicates a 6-fold increase in shear strain (and therefore average strain rate) within the mylonites, assuming ~~that the~~ a homogeneous distribution of strain and constant relative displacement across the Woodroffe Thrust ~~was constant~~thickness along the entire ca. 60 km transect. This trend from south to north is accompanied by a slight decrease in metamorphic temperature of ca. 100 °C ~~(Wex et al., 2017)~~(Wex et al., 2017) and the shift from "dry" to "wet" conditions, as reflected in the increasing abundance of hydrous minerals (Fig. ~~10~~9). The thickness

of large-scale shear zones is considered to decrease with decreasing temperature and depth (Platt and Behr, 2011a, 2011b) and displacement (Hull, 1988)~~, but may also decrease with increasing fluid-rock interaction as a consequence of volume loss (e.g., Newman and Mitra, 1993).~~. A point in the footwall only enters the shear zone when it passes the toe of the thrust (that is where the thrust meets the surface). This could potentially lead to a variation in the finite shear strain experienced in the footwall. However, the whole of the exposed ca. 60 km N-S section was formerly at mid- to lower crustal level (Wex et al., 2017) and thus nowhere near the thrust toe. There is also currently no evidence for major splays of the Woodroffe Thrust into the hanging wall. ~~We therefore assume that the studied section experienced more or less the same relative displacement and that variation in this parameter cannot~~Distributed folding related to the Peterman Orogeny is observable on the regional scale in the footwall (Wex et al., 2017) but the amount of shortening involved cannot be quantified. It follows that there is presently no indication for a significant change in relative displacement along the studied section and that variation in this parameter therefore cannot be used to account for the difference in mylonite thickness. It was argued above that the greater abundance of hydrous minerals in the footwall Mulga Park Subdomain compared to the hanging wall Fregon Subdomain, reflecting peak metamorphic conditions of upper amphibolite facies and granulite facies respectively during the earlier Musgravian Orogeny, resulted in slightly "wetter" conditions in the footwall during activity of the Woodroffe Thrust. This was proposed as an explanation for the broader zone of mylonites in the footwall~~, which in turn would argue against the increasingly hydrous conditions toward the north as an explanation for the decrease in overall mylonite width. The general decrease in mylonite zone thickness toward the north is therefore interpreted to be due to the established decrease in metamorphic temperature, promoting localization in a narrower zone~~. However, it creates the apparent contradiction that the thickness of the mylonitic zone decreases with increasing water activity to the north. Such an observation might reflect the possibility that even a small amount of fluid was able to weaken the footwall relative to the strong "drier" hanging wall, allowing it to preferentially take up deformation because of its lower effective viscosity. An increase in the water content to the north would result in an increase of the effective viscosity ratio between footwall and hanging wall, yielding a stronger localization toward the interface and a narrower mylonite zone that extends less into the stronger material. This hypothesis is supported by the current observations in this paper, but there is not yet a theoretical basis to provide a full explanation. Decreasing temperature to the north could also lead to increased localization and decreased shear zone thickness, both directly (Platt and Behr, 2011a, 2011b) and as a second order effect that accentuates the strength contrast as both footwall and hanging wall become stronger with decreasing temperature. Water activity thus seems to be the crucial factor controlling both the preferential development of mylonites in the footwall and the decrease in thickness with increasing water activity towards the north.

9 Conclusions

Field and thin section observations establish that the rocks of the central Musgrave Block were predominantly "dry" during development of the midcrustal Woodroffe Thrust during the ca. 560-520 Ma Petermann Orogeny, but with a progression in the thrust direction towards locally "wet" conditions in some of the northernmost exposures. This is indicated by: (1) rare occurrence of syntectonic quartz veins and quartz-rich pegmatites (locally found only in the north), (2) metastability of

plagioclase in the presence of K-feldspar, which rarely shows significant ~~sericitization~~alteration via the reaction An + Or + H_2O = Ms + Ep + Qz (more common towards the north) and (3) preferential high-pressure breakdown of plagioclase via the reaction An = Grs + Ky + Qz (common in the southerly exposures), rather than An + H_2O = Ep + Ky + Qz. Aqueous fluids were most likely derived internally from hydrous minerals within the footwall gneisses and granitoids, implying that the rocks in the study area were a relatively closed system.

The thickness of the Woodroffe Thrust mylonites generally increases with increasing metamorphic grade and ~~does not appear to be linked to the presence or absence of an aqueous fluid. However, atypical~~decreasing availability of aqueous fluids. Atypical of a thrust, ductile deformation is more extensively developed in the footwall rocks and only marginally involved several tens of metres of the lowermost hanging wall. The inverse gradient of ductile deformation cannot be explained by thermal weakening or the distributed presence of pseudotachylyte (acting as preferred nucleation sites for shearing), but rather by preferential ~~water assisted~~rheological weakening ~~in~~of the "wetter" footwall compared to the "~~dry~~drier" hanging wall. This reflects the earlier (Musgravian Orogeny) peak metamorphic conditions (granulite facies in the hanging wall and upper amphibolite facies in the footwall) and the contrasting availability of aqueous fluids derived from relict hydrous minerals in the footwall and hanging wall.

Data availability

Supplementary data are available in the Supporting Information "S1" to "S5" and further information can be obtained on request from the corresponding author.

Competing interests

The authors declare that they have no conflict of interest.

Author contribution

Each of the listed authors took part in at least two of three field seasons, which formed the basis of this study. Alfredo Camacho's previous knowledge of the Musgrave Ranges and the local communities was essential for the success of the campaign. Neil Mancktelow and Giorgio Pennacchioni developed the initial idea of the study. Sebastian Wex prepared the manuscript with contributions from all co-authors.

Acknowledgments

We thank the communities of the Anangu Pitjantjatjara Yankunytjatjara Lands (APY) for granting us access to the Musgrave Ranges. Logistical support from the Northern Territory Geological Survey (NTGS) of Australia, ~~Prof. B.~~Basil Tikoff (Univ. Wisconsin, Madison) and Shane and Alethea Nicolle are gratefully recognized. We further acknowledge the support of ~~Dr. K.~~Karsten Kunze from the Scientific Center for Optical and Electron Microscopy (ScopeM) at the ETH, Zurich. ~~Dr. J.~~Jost Eikenberg is thanked for supervising and conducting the thorium measurements at the Paul Scherrer Institute (PSI) in Villigen, Switzerland. We further acknowledge the support of ~~M.~~Madalina Jaggi who carried out the stable isotope analyses at the Geological Institute at ETH, Zurich. This project was financed by the Swiss National Science Foundation (SNF) Grant 200021_146745 ~~and by~~awarded to Neil Mancktelow, with additional funding from the University of Padova (BIRD175145/17: The geological record of deep earthquakes: the association pseudotachylyte-mylonite~~).~~) awarded to Giorgio Pennacchioni.

References

Allen, J. L. and Shaw, C. A.: Seismogenic structure of a crystalline thrust fault: fabric anisotropy and coeval pseudotachylyte-mylonitic pseudotachylyte in the Grizzly Creek Shear Zone, Colorado, in: Geology of the Earthquake Source: A Volume in Honour of Rick Sibson, edited by A. Fagereng, V. G. Toy, and J. V. Rowland, pp. 135–151, Geol. Soc. Spec. Publ., 359, London, 2011.

Andersen, T. B. and Austrheim, H.: Fossil earthquakes recorded by pseudotachylytes in mantle peridotite from the Alpine subduction complex of Corsica, Earth Planet. Sci. Lett., 242(1–2), 58–72, doi:10.1016/j.epsl.2005.11.058, 2006.

Austrheim, H. and Andersen, T. B.: Pseudotachylytes from Corsica: fossil earthquakes from a subduction complex, Terra Nov., 16(4), 193–197, doi:10.1111/j.1365-3121.2004.00551.x, 2004.

Ballhaus, C. and Glikson, A. Y.: The petrology of layered mafic-ultramafic intrusions of the Giles complex, western Musgrave Block, Western Australia, AGSO J. Aust. Geol. Geophys., 16(1/2), 69–90, 1995.

Bell, T. H.: Progressive deformation and reorientation of fold axes in a ductile mylonite zone: The Woodroffe Thrust, Tectonophysics, 44(1–4), 285–320, doi:10.1016/0040-1951(78)90074-4, 1978.

Bell, T. H. and Etheridge, M. A.: The deformation and recrystallization of quartz in a mylonite zone, central Australia, Tectonophysics, 32(3–4), 235–267, doi:10.1016/0040-1951(76)90064-0, 1976.

Bell, T. H. and Johnson, S. E.: The role of deformation partitioning in the deformation and recrystallization of plagioclase and K-feldspar in the Woodroffe Thrust mylonite zone, central Australia, J. Metamorph. Geol., 7(2), 151–168, doi:10.1111/j.1525-1314.1989.tb00582.x, 1989.

Bell, T. H. and Johnson, S. E.: Shear sense: a new approach that resolves conflicts between criteria in metamorphic rocks, J. Metamorph. Geol., 10(1), 99–124, doi:10.1111/j.1525-1314.1992.tb00074.x, 1992.

Berglund, M. and Wieser, M. E.: Isotopic compositions of the elements 2009 (IUPAC Technical Report), Pure Appl. Chem., 83(2), 397–410, doi:10.1351/PAC-REP-10-06-02, 2011.

Boyd, F. R. and England, J. L.: Melting of silicates at high pressures, in: Carnegie Inst. Wash. Yr. Book 60, pp. 113–125, Port City Press, Baltimore, 1961.

Breitenbach, S. F. M. and Bernasconi, S. M.: Carbon and oxygen isotope analysis of small carbonate samples (20 to 100 µg) with a GasBench II preparation device, Rapid Commun. Mass Spectrom., 25(13), 1910–1914, doi:10.1002/rcm.5052, 2011.

Camacho, A.: An Isotopic Study of Deep-Crustal Orogenic Processes: Musgrave Block, Central Australia, PhD Thesis. The Australian National University, Canberra, 261 pp., 1997.

Camacho, A. and Fanning, C. M.: Some isotopic constraints on the evolution of the granulite and upper amphibolite facies terranes in the eastern Musgrave Block, central Australia, Precambrian Res., 71(1–4), 155–181, doi:10.1016/0301-9268(94)00060-5, 1995.

Camacho, A. and McDougall, I.: Intracratonic, strike-slip partitioned transpression and the formation and exhumation of eclogite facies rocks: An example from the Musgrave Block, central Australia, Tectonics, 19(5), 978–996, doi:10.1029/1999TC001151, 2000.

Camacho, A., Simons, B. and Schmidt, P. W.: Geological and palaeomagnetic significance of the Kulgera Dyke Swarm, Musgrave Block, NT, Australia, Geophys. J. Int., 107(1), 37–45, doi:10.1111/j.1365-246X.1991.tb01154.x, 1991.

Camacho, A., Vernon, R. H. and Fitz Gerald, J. D.: Large volumes of anhydrous pseudotachylyte in the Woodroffe Thrust, eastern Musgrave Ranges, Australia, J. Struct. Geol., 17(3), 371–383, doi:10.1016/0191-8141(94)00069-C, 1995.

Camacho, A., Compston, W., McCulloch, M. and McDougall, I.: Timing and exhumation of eclogite facies shear zones, Musgrave Block, central Australia, J. Metamorph. Geol., 15(6), 735–751, doi:10.1111/j.1525-1314.1997.00053.x, 1997.

Camacho, A., Yang, P. and Frederiksen, A.: Constraints from diffusion profiles on the duration of high-strain deformation in thickened crust, Geology, 37(8), 755–758, doi:10.1130/G25753A.1, 2009.

Camacho, A., Armstrong, R., Davis, D. W. and Bekker, A.: Early history of the Amadeus Basin: Implications for the existence and geometry of the Centralian Superbasin, Precambrian Res., 259, 232–242, doi:10.1016/j.precamres.2014.12.004, 2015.

Chacko, T., Mayeda, T. K., Clayton, R. N. and Goldsmith, J. R.: Oxygen and carbon isotope fractionations between CO_2 and calcite, Geochim. Cosmochim. Acta, 55(10), 2867–2882, doi:10.1016/0016-7037(91)90452-B, 1991.

~~Chatterjee, N. D., Johannes, W. and Leistner, H.: The system CaO-Al_2O_3-SiO_2-H_2O: new phase equilibria data, some calculated phase relations, and their petrological applications, Contrib. to Mineral. Petrol., 88(1–2), 1–13, doi:10.1007/BF00371407, 1984.~~

Christie, J. M.: Moine Thrust Zone in the Assynt region of northwest Scotland, Univ. Calif. Publ. Geol. Sci., 40(6), 345–440, 1963.

Clarke, G. L., Buick, I. S., Glikson, A. Y. and Stewart, A. J.: Structural and pressure-temperature evolution of host rocks of the Giles Complex, western Musgrave Block, central Australia: evidence for multiple high-pressure events, AGSO J. Aust. Geol. Geophys., 16(1/2), 127–146, 1995.

Collerson, K. D., Oliver, R. L. and Rutland, R. W. R.: An example of structural and metamorphic relationships in the Musgrave orogenic belt, central Australia, J. Geol. Soc. Aust., 18(4), 379–393, doi:10.1080/00167617208728776, 1972.

Cooper, A. F. and Norris, R. J.: Anatomy, structural evolution, and slip rate of a plate boundary thrust: The Alpine Fault at Gaunt Creek, Westland, New Zealand, Geol. Soc. Am. Bull., 106(5), 627–633, doi:10.1130/0016-7606(1994)106<0627:ASEASR>2.3.CO;2, 1994.

Coplen, T. B., Böhlke, J. K., De Bièvre, P., Ding, T., Holden, N. E., Hopple, J. A., Krouse, H. R., Lamberty, A., Peiser, H. S., Révész, K., Rieder, S. E., Rosman, K. J. R., Roth, E., Taylor, P. D. P., Vocke, R. D. and Xiao, Y. K.: Isotope-abundance variations of selected elements (IUPAC Technical Report), Pure Appl. Chem., 74(10), 1987–2017, doi:10.1351/pac200274101987, 2002.

Coward, M. P.: The Caledonian thrust and shear zones of N.W. Scotland, J. Struct. Geol., 2(1–2), 11–17, doi:10.1016/0191-8141(80)90029-2, 1980.

Davis, G. A.: Rapid upward transport of mid-crustal mylonitic gneisses in the footwall of a Miocene detachment fault, Whipple Mountains, southeastern California, Geol. Rundschau, 77(1), 191–209, doi:10.1007/BF01848684, 1988.

Davis, G. A. and Lister, G. S.: Detachment faulting in continental extension; Perspectives from the Southwestern U.S. Cordillera, Geol. Soc. Am. Spec. Pap., 218, 133–159, doi:10.1130/SPE218-p133, 1988.

Deines, P.: The carbon isotope geochemistry of mantle xenoliths, Earth-Science Rev., 58(3–4), 247–278, doi:10.1016/S0012-8252(02)00064-8, 2002.

Edgoose, C. J., Camacho, A., Wakelin-King, G. A. and Simons, B. A.: 1:250 000 Geological Map Series Explanatory Notes. Kulgera SG 53-5, 2nd ed., North. Territ. Geol. Surv., Darwin, 1993.

Edgoose, C. J., Scrimgeour, I. R. and Close, D. F.: Report 15: Geology of the Musgrave Block, Northern Territory, North. Territ. Geol. Surv., Darwin, 2004.

Eikenberg, J.: Radium Isotope Systematics in Nature: Applications in Geochronology and Hydrogeochemistry, Habilitation Thesis. Devision for Radiation Safety and Security, Paul Scherrer Institute (PSI), Villigen, Switzerland and Earth Science Department, Swiss Federal Institute of Technology (ETH), Zurich, 193 pp., 2002.

Ellis, D. J. and Maboko, M. A. H.: Precambrian tectonics and the physicochemical evolution of the continental crust. I. The gabbro-eclogite transition revisited, Precambrian Res., 55(1–4), 491–506, doi:10.1016/0301-9268(92)90041-L, 1992.

Evins, P. M., Smithies, R. H., Howard, H. M., Kirkland, C. L., Wingate, M. T. D. and Bodorkos, S.: Record 2010/6: Redefining the Giles Event within the setting of the 1120-1020 Ma Ngaanyatjarra Rift, west Musgrave Province, central Australia, Geol. Surv. West. Aust., Perth, 2010.

Fitz Gerald, J. D., Mancktelow, N. S., Pennacchioni, G. and Kunze, K.: Ultra-fine grained quartz mylonites from high-grade shear zones: Evidence for strong dry middle to lower crust, Geology, 34(5), 369–372, doi:10.1130/G22099.1, 2006.

Flottmann, T., Hand, M., Close, D., Edgoose, C. and Scrimgeour, I.: Thrust Tectonic Styles of the Intracratonic Alice Springs and Petermann Orogenies, Central Australia, in: AAPG Memoir 82: Thrust tectonics and hydrocarbon systems, edited by K. R. McClay, pp. 538–557, Tulsa, 2004.

Forman, D. J.: 1:250,000 Geological Series Explanatory Notes. Ayers Rock, N.T. SG/52-8, 1st ed., Bur. Miner. Resour. Geol. Geophys., Canberra, 1965.

675 Fossen, H. and Cavalcante, G. C. G.: Shear zones – A review, Earth-Science Rev., 171, 434–455, doi:10.1016/j.earscirev.2017.05.002, 2017.

Goldsmith, J. R.: The melting and breakdown reactions of anorthite at high pressures and temperatures, Am. Mineral., 65(3–4), 272–284, 1980.

Goldsmith, J. R.: Plagioclase stability at elevated temperatures and water pressures., Am. Mineral., 67(7–8), 653–675, 1982.

680 Gray, C. M.: The Geochemistry of Central Australian Granulites in Relation to the Chemical and Isotopic Effects of Granulite Facies Metamorphism, Contrib. to Mineral. Petrol., 65(1), 79–89, doi:10.1007/BF00373573, 1977.

Gray, C. M.: Geochronology of granulite-facies gneisses in the western Musgrave Block, central Australia, J. Geol. Soc. Aust., 25(7), 403–414, doi:10.1080/00167617808729050, 1978.

Gray, C. M. and Compston, W.: A rubidium-strontium chronology of the metamorphism and prehistory of central Australian

685 granulites, Geochim. Cosmochim. Acta, 42(11), 1735–1747, doi:10.1016/0016-7037(78)90259-4, 1978.

Griggs, D.: Hydrolytic Weakening of Quartz and Other Silicates, Geophys. J. R. Astron. Soc., 14(1–4), 19–31, doi:10.1111/j.1365-246X.1967.tb06218.x, 1967.

Griggs, D.: A Model of Hydrolytic Weakening in Quartz, J. Geophys. Res., 79(11), 1653–1661, doi:10.1029/JB079i011p01653, 1974.

690 Griggs, D. T. and Blacic, J. D.: Quartz: Anomalous Weakness of Synthetic Crystals, Science, 147(3655), 292–295, doi:10.1126/science.147.3655.292, 1965.

Handy, M. R., Hirth, G. and Bürgmann, R.: Continental fault structure and rheology from the frictional-to-viscous transition downward, in: Tectonic Faults: Agents of Change on a Dynamic Earth, edited by M. R. Handy, G. Hirth, and N. Hovius, pp. 139–181, MIT Press, Cambridge, 2007.

695 Hariya, Y. and Kennedy, G. C.: Equilibrium study of anorthite under high pressure and high temperature, Am. J. Sci., 266(3), 193–203, doi:10.2475/ajs.266.3.193, 1968.

Hawemann, F., Mancktelow, N., Wex, S., Camacho, A. and Pennacchioni, G.: Strain localization on different scales and the importance of brittle precursors during deformation in the lower crust (Davenport Shear Zone, Central Australia), Geophys. Res. Abstr., 16, 5009, 2014.

700 Hawemann, F., Mancktelow, N. S., Wex, S., Camacho, A. and Pennacchioni, G.: Pseudotachylyte as field evidence for lower crustal earthquakes during the intracontinental Petermann Orogeny (Musgrave Block, Central Australia), Solid Earth Discuss., in review, doi:10.5194/se-2017-123, 2017.

Heier, K. S. and Adams, J. A. S.: Concentration of radioactive elements in deep crustal material, Geochim. Cosmochim. Acta, 29(1), 53–61, doi:doi.org/10.1016/0016-7037(65)90078-5, 1965.

705 Hill, A. C., Arouri, K., Gorjan, P. and Walter, M. R.: Geochemistry of marine and nonmarine environments of a Neoproterozoic cratonic carbonate/evaporite: the Bitter Springs Formation, central Australia, in: Carbonate Sedimentation and Diagenesis in the Evolving Precambrian World, edited by J. P. Grotzinger and N. P. James, pp. 327–344, SEPM (Soc. Sediment. Geol.) Spec. Publ., 67, Tulsa, 2000.

Hobbs, B. E.: The hydrolytic weakening effect in quartz, in: Point Defects in Minerals, edited by R. N. Schock, pp. 151–170, Am. Geophys. Union, Geophys. Monogr. Ser., 31, Washington D.C., 1985.

Hull, J.: Thickness-displacement relationships for deformation zones, J. Struct. Geol., 10(4), 431–435, doi:10.1016/0191-8141(88)90020-X, 1988.

Javoy, M., Pineau, F. and Delorme, H.: Carbon and nitrogen isotopes in the mantle, Chem. Geol., 57(1–2), 41–62, doi:10.1016/0009-2541(86)90093-8, 1986.

Kretz, R.: Note on some equilibria in which plagioclase and epidote participate, Am. J. Sci., 261(10), 973–982, doi:10.2475/ajs.261.10.973, 1963.

Kronenberg, A. K., Segall, P. and Wolf, G. H.: Hydrolytic Weakening and Penetrative Deformation Within a Natural Shear Zone, in: The Brittle-Ductile Transition in Rocks, edited by A. G. Duba, W. B. Durham, J. W. Handin, and H. F. Wang, pp. 21–36, Am. Geophys. Union, Geophys. Monogr. Ser., 56, Washington D.C., 1990.

Lambert, I. B. and Heier, K. S.: The vertical distribution of uranium, thorium and potassium in the Continental Crust, Geochim. Cosmochim. Acta, 31(3), 377–390, doi:10.1016/0016-7037(67)90048-8, 1967.

Lambert, I. B. and Heier, K. S.: Geochemical investigations of deep-seated rocks in the Australian shield, Lithos, 1(1), 30–53, doi:10.1016/S0024-4937(68)80033-7, 1968.

Lin, A., Maruyama, T., Aaron, S., Michibayashi, K., Camacho, A. and Kano, K.: Propagation of seismic slip from brittle to ductile crust: Evidence from pseudotachylyte of the Woodroffe thrust, central Australia, Tectonophysics, 402(1–4), 21–35, doi:10.1016/j.tecto.2004.10.016, 2005.

Lund, M. G. and Austrheim, H.: High-pressure metamorphism and deep-crustal seismicity: evidence from contemporaneous formation of pseudotachylytes and eclogite facies coronas, Tectonophysics, 372(1–2), 59–83, doi:10.1016/S0040-1951(03)00232-4, 2003.

Maboko, M. A. H., McDougall, I. and Zeitler, P. K.: Metamorphic P-T path of granulites in the Musgrave Ranges, central Australia, in: Evolution of Metamorphic Belts, edited by J. S. Daly, R. A. Cliff, and B. W. D. Yardley, pp. 303–307, Geol. Soc. Spec. Publ., 43, London, 1989.

Maboko, M. A. H., Williams, I. S. and Compston, W.: Zircon U-Pb Chronometry of the Pressure and Temperature History of Granulites in the Musgrave Ranges, Central Australia, J. Geol., 99(5), 675–697, 1991.

Maboko, M. A. H., McDougall, I., Zeitler, P. K. and Williams, I. S.: Geochronological evidence for ~ 530-550 Ma juxtaposition of two Proterozoic metamorphic terranes in the Musgrave Ranges, central Australia, Aust. J. Earth Sci., 39(4), 457–471, doi:10.1080/08120099208728038, 1992.

Major, R. B.: Woodroffe Thrust Zone in the Musgrave Ranges, Q. Geol. Notes, 35, 9–11, 1970.

Major, R. B.: Explanatory Notes for the Woodroffe 1:250 000 Geological Map SG/52-12, 1st ed., Geol. Surv. South Aust., Adelaide, 1973.

Major, R. B. and Conor, C. H. H.: Musgrave Block, in: Bulletin 54: The geology of South Australia. Volume 1. The Precambrian, edited by J. F. Drexel, W. V. Preiss, and A. J. Parker, pp. 156–167, Geol. Surv. South Aust., Adelaide, 1993.

Major, R. B., Johnson, J. E., Leeson, B., Mirams, R. C. and Thomson, B. P.: 1:250 000 S. A. Geological Atlas Series Sheet. Woodroffe SG 52-12 Zone 4., 1st ed., Geol. Surv. South Aust., Adelaide, 1967.

Mancktelow, N.: The Simplon Line: a major displacement zone in the western Lepontine Alps, Eclogae Geol. Helv., 78(1), 73–96, doi:10.5169/seals-165644, 1985.

Mancktelow, N. S. and Pennacchioni, G.: The influence of grain boundary fluids on the microstructure of quartz-feldspar mylonites, J. Struct. Geol., 26(1), 47–69, doi:10.1016/S0191-8141(03)00081-6, 2004.

Mancktelow, N. S. and Pennacchioni, G.: The control of precursor brittle fracture and fluid-rock interaction on the development of single and paired ductile shear zones, J. Struct. Geol., 27(4), 645–661, doi:10.1016/j.jsg.2004.12.001, 2005.

Menegon, L., Pennacchioni, G., Malaspina, N., Harris, K. and Wood, E.: Earthquakes as Precursors of Ductile Shear Zones in the Dry and Strong Lower Crust, Geochemistry, Geophys. Geosystems, 18, 4356–4374, doi:10.1002/2017GC007189, 2017.

Milke, R., Neusser, G., Kolzer, K. and Wunder, B.: Very little water is necessary to make a dry solid silicate system wet, Geology, 41(2), 247–250, doi:10.1130/G33674.1, 2013.

~~Newman, J. and Mitra, G.: Lateral variations in mylonite zone thickness as influenced by fluid-rock interactions, Linville Falls fault, North Carolina, J. Struct. Geol., 15(7), 849–863, doi:10.1016/0191-8141(93)90180-I, 1993.~~

Myers, J. S., Shaw, R. D. and Tyler, I. M.: Tectonic evolution of Proterozoic Australia, Tectonics, 15(6), 1431–1446, doi:10.1029/96TC02356, 1996.

Passchier, C. W.: Pseudotachylyte and the development of ultramylonite bands in the Saint-Barthélemy Massif, French Pyrenees, J. Struct. Geol., 4(1), 69–79, doi:10.1016/0191-8141(82)90008-6, 1982.

Passchier, C. W.: Mylonite-dominated footwall geometry in a shear zone, central Pyrenees, Geol. Mag., 121(5), 429–436, doi:10.1017/S0016756800029964, 1984.

Passchier, C. W. and Trouw, R. A. J.: Microtectonics, 2nd ed., Springer, Berlin, Heidelberg, 2005.

Pennacchioni, G. and Cesare, B.: Ductile-brittle transition in pre-Alpine amphibolite facies mylonites during evolution from water-present to water-deficient conditions (Mont Mary nappe, Italian Western Alps), J. Metamorph. Geol., 15(6), 777–791, doi:10.1111/j.1525-1314.1997.00055.x, 1997.

Percival, P. J.: Record 2010/13: Index of Airborne Geophysical Surveys, 11th ed., Geoscience Australia, Canberra, 2010.

Pittarello, L., Pennacchioni, G. and Di Toro, G.: Amphibolite-facies pseudotachylytes in Premosello metagabbro and felsic mylonites (Ivrea Zone, Italy), Tectonophysics, 580, 43–57, doi:10.1016/j.tecto.2012.08.001, 2012.

Platt, J. P. and Behr, W. M.: Deep structure of lithospheric fault zones, Geophys. Res. Lett., 38(24), 1–6, doi:10.1029/2011GL049719, 2011a.

Platt, J. P. and Behr, W. M.: Lithospheric shear zones as constant stress experiments, Geology, 39(2), 127–130, doi:10.1130/G31561.1, 2011b.

Ramberg, H.: The Facies Classification of Rocks: A Clue to the Origin of Quartzo-Feldspathic Massifs and Veins, J. Geol., 57(1), 18–54, doi:10.1086/625573, 1949.

Schmidt, P. W., Williams, G. E., Camacho, A. and Lee, J. K. W.: Assembly of Proterozoic Australia: Implications of a revised

pole for the ~1070 Ma Alcurra Dyke Swarm, central Australia, Geophys. J. Int., 167(2), 626–634, doi:10.1111/j.1365-246X.2006.03192.x, 2006.

Scrimgeour, I. and Close, D.: Regional high-pressure metamorphism during intracratonic deformation: The Petermann Orogeny, central Australia, J. Metamorph. Geol., 17(5), 557–572, doi:10.1046/j.1525-1314.1999.00217.x, 1999.

Scrimgeour, I. R., Close, D. F. and Edgoose, C. J.: 1:250,000 Geological Map Series and Explanatary Notes. Petermann Ranges SG52-7, 2nd ed., North. Territ. Geol. Surv., Darwin, 1999.

Selverstone, J., Axen, G. J. and Luther, A.: Fault localization controlled by fluid infiltration into mylonites: Formation and strength of low-angle normal faults in the midcrustal brittle-plastic transition, J. Geophys. Res., 117, B06210, doi:10.1029/2012JB009171, 2012.

Sibson, R. H., White, S. H. and Atkinson, B. K.: Structure and distribution of fault rocks in the Alpine Fault Zone, New Zealand, in: Thrust and Nappe Tectonics, edited by K. R. McClay and N. J. Price, pp. 197–210, Geol. Soc. Spec. Publ., 9, London, 1981.

Smithies, R. H., Howard, H. M., Evins, P. M., Kirkland, C. L., Kelsey, D. E., Hand, M., Wingate, M. T. D., Collins, A. S. and Belousova, E.: High-Temperature Granite Magmatism, Crust-Mantle Interaction and the Mesoproterozoic Intracontinental Evolution of the Musgrave Province, Central Australia, J. Petrol., 52(5), 931–958, doi:10.1093/petrology/egr010, 2011.

Sprigg, R. C., Wilson, B., Coats, R. P., Webb, B. P. and O'Driscoll, E. S.: 4 Mile Geological Series Sheet. Alberga G 53-9 Zone 4, 1st ed., Geol. Surv. South Aust., Adelaide, 1959.

Stewart, A. J.: Western extension of the Woodroffe Thrust, Musgrave Block, central Australia, AGSO J. Aust. Geol. Geophys., 16(1/2), 147–153, 1995.

Stewart, A. J.: Record 1997/5: Geology of the Bates 1:100 000 Sheet Area (4646), Musgrave Block, Western Australia, 1st ed., Aust. Geol. Surv. Organ., Canberra, 1997.

Stünitz, H., Thust, A., Heilbronner, R., Behrens, H., Kilian, R., Tarantola, A. and Fitz Gerald, J. D.: Water redistribution in experimentally deformed natural milky quartz single crystals - Implications for H_2O-weakening processes, J. Geophys. Res. Solid Earth, 122(2), 866–894, doi:10.1002/2016JB013533, 2017.

Sun, S. and Sheraton, J.: Zircon U/Pb chronology, tectono-thermal and crust-forming events in the Tomkinson Ranges, Musgrave Block, Central Australia, AGSO Res. Newsl., 17, 9–11, 1992.

Sun, S., Sheraton, J. W., Glikson, A. Y. and Stewart, A. J.: A major magmatic event during 1050-1080 Ma in central Australia, and an emplacement age for the Giles Complex, AGSO Res. Newsl., 24, 13–15, 1996.

Taylor, H. P.: Oxygen and Hydrogen Isotope Relationships in Hydrothermal Mineral Deposits, in: Geochemistry of Hydrothermal Ore Deposits, edited by H. L. Barnes, pp. 229–302, John Wiley and Sons, New York, 1997.

Tucker, N. M. T., Hand, M., Kelsey, D. E. and Dutch, R. A.: A duality of timescales: Short-lived ultrahigh temperature metamorphism preserving a long-lived monazite growth history in the Grenvillian Musgrave–Albany–Fraser Orogen, Precambrian Res., 264, 204–234, doi:10.1016/j.precamres.2015.04.015, 2015.

Tullis, J. and Yund, R. A.: Hydrolytic weakening of quartz aggregates: The effects of water and pressure on recovery, Geophys.

Res. Lett., 16(11), 1343–1346, doi:10.1029/GL016i011p01343, 1989.

Walsh, A. K., Kelsey, D. ., Kirklan, C. L., Hand, M., Smithies, R. H., Clark, C. and Howard, H. M.: P–T–t evolution of a large, long-lived, ultrahigh-temperature Grenvillian belt in central Australia, Gondwana Res., 28(2), 531–564, doi:10.1016/j.gr.2014.05.012, 2015.

Wayte, G. J., Worden, R. H., Rubie, D. C. and Droop, G. T. R.: A TEM study of disequilibrium plagioclase breakdown at high pressure: the role of infiltrating fluid, Contrib. to Mineral. Petrol., 101(4), 426–437, doi:10.1007/BF00372216, 1989.

Wells, A. T., Forman, D. J., Ranford, L. C. and Cook, P. J.: Bulletin 100: Geology of the Amadeus Basin, Central Australia, Bur. Miner. Resour. Geol. Geophys., Canberra, 1970.

Wex, S., Mancktelow, N., Hawemann, F., Camacho, A. and Pennacchioni, G.: Pseudotachylyte formation vs. mylonitization - repeated cycles of seismic fracture and aseismic creep in the middle crust (Woodroffe Thrust, Central Australia), Geophys. Res. Abstr., 16, 5071, 2014.

Wex, S., Mancktelow, N. S., Hawemann, F., Camacho, A. and Pennacchioni, G.: Geometry of a large-scale, low-angle, midcrustal thrust (Woodroffe Thrust, central Australia), Tectonics, 36(11), 2447–2476, doi:10.1002/2017TC004681, 2017.

Whitney, D. L. and Evans, B. W.: Abbreviations for names of rock-forming minerals, Am. Mineral., 95(1), 185–187, doi:10.2138/am.2010.3371, 2010.

Young, D. N., Duncan, N., Camacho, A., Ferenczi, P. A. and Madigan, T. L. A.: 1:250 000 Geological Map Series and Explanatory Notes. Ayers Rock SG 52-8, 2nd ed., North. Territ. Geol. Surv., Darwin, 2002.

Zhao, J. and McCulloch, M. T.: Sm-Nd mineral isochron ages of Late Proterozoic dyke swarms in Australia: evidence for two distinctive events of mafic magmatism and crustal extension, Chem. Geol., 109(1–4), 341–354, doi:10.1016/0009-2541(93)90079-X, 1993.

Zhao, J., McCulloch, M. T. and Korsch, R. J.: Characterisation of a plume-related ~ 800 Ma magmatic event and its implications for basin formation in central-southern Australia, Earth Planet. Sci. Lett., 121(3–4), 349–367, doi:10.1016/0012-821X(94)90077-9, 1994.

S1 Methodology

S1.1 Scanning electron microscopy (SEM)

Backscattered electron (BSE, atomic Z-contrast) analysis was performed using an FEI Quanta 200F scanning electron microscope equipped with a field emission gun at the Scientific Center for Optical and Electron Microscopy (ScopeM) at ETH, Zurich. BSE settings were: acceleration voltage 10-20 kV, working distance 10 mm, aperture 3-4, spot size 4 and high vacuum. Thin sections were carbon-coated.

S1.2 γ-ray spectrometry (^{232}Th)

Trace concentrations of thorium in felsic gneisses and granitoids have been measured using γ-ray spectrometry. This method, rather than laser ablation inductively coupled plasma mass spectrometry (LA-ICP-MS), was applied, because it does not require extensive sample preparation and represents a quick and efficient method of acquiring the desired element concentration.

Thorium-232 accounts for 100 % of the element's natural abundance (Berglund and Wieser, 2011). Therefore, a sample's thorium content was assessed by quantifying the activity of this particular radioactive thorium isotope. Thorium-232 was not measured directly because it is a pure α-emitter without photon emission (Fig. S1). However, due to the Mesoproterozoic age (ca. 1200 Ma) of the deformation event (Musgravian Orogeny) which produced the contrasting thorium concentrations in the hanging wall and footwall of the Woodroffe Thrust, all products of the thorium-232 decay series (Fig. S1) can be assumed to be in equilibrium (secular equilibrium in the thorium series is obtained after only 30 years). As a consequence, the activity of thorium-232 and all daughter isotopes is the same. Thus, the thorium concentration can be indirectly measured via the γ-decay of the shorter-lived radium-228. The five most important peaks related to the γ-decay of radium-228 are located at 77.1 keV, 238.6 keV, 338.4 keV, 583.2 keV, 911.1 keV in the energy spectrum (Fig. S2). Measurements were conducted on thin section chips (weights ranging between 14-42 g) using γ-ray spectrometers at the Paul Scherrer Institute (PSI) in Villigen, Switzerland with a default measurement time of two hours. If the aspired error (2 x standard deviation) of 10 % was achieved earlier (thorium-rich samples), the measurement was stopped, otherwise it was run overnight for up to 15 hours (thorium-poor samples). Results were weight-averaged, with the highest significance being attributed to the strongest peak at 238.6 keV, in order to obtain the activity of radium-228 normalized to sample weight (Bq/kg). Following up on the assumption that the activity of thorium-232 and radium-228 are the same, this value was divided by the specific activity of thorium-232 (4060 Bq/g; Eikenberg, 2002) in order to obtain the concentration of thorium-232. The detection limit was determined from the 238.6 keV peak of lead-212. All measurements were done assuming a three centimetre plane source as sample geometry. Due to the dependence of the detector efficiency on the geometry and especially the thickness of each thin section chip, a correction factor was applied. This correction factor is equal to the relative difference between the detector efficiency of each sample with respect to the three centimetre plane source. All thin section chips were grouped according to their geometry and thickness and for each group a representative sample was chosen and the correction factor determined using a Monte Carlo approach.

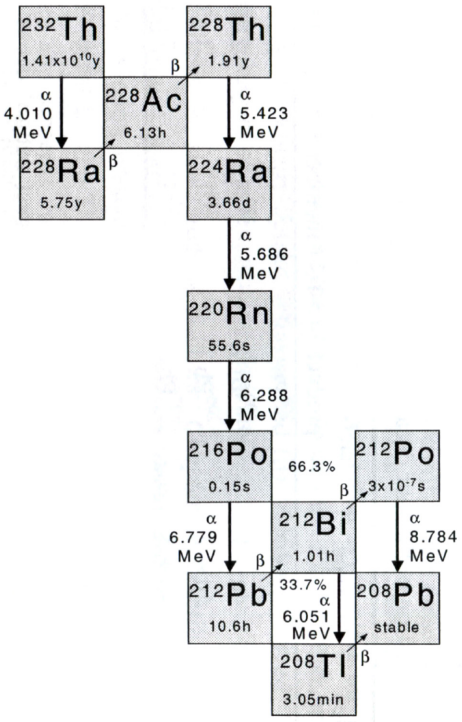

40 **Figure S1: Schematic illustration of the thorium-232 decay series members. For simplicity of the scheme, in comparison to standard isotope tables, neutrons are not considered. From Eikenberg (2002).**

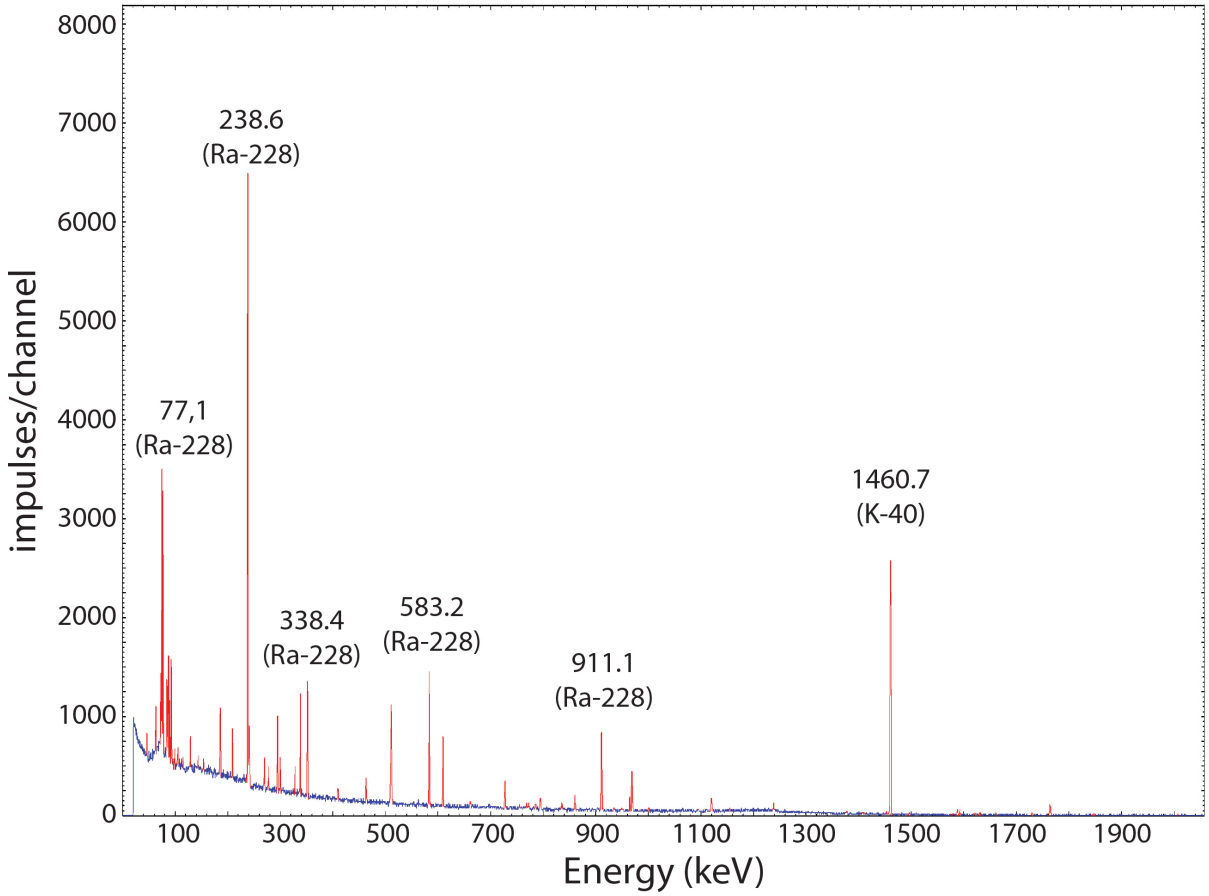

Figure S2: γ-spectrum of radium-228 with the most relevant energy peaks highlighted. Sample SW13-323A (coordinates: 132.14344, -25.99211; location 6 in Fig. 1 of the main paper).

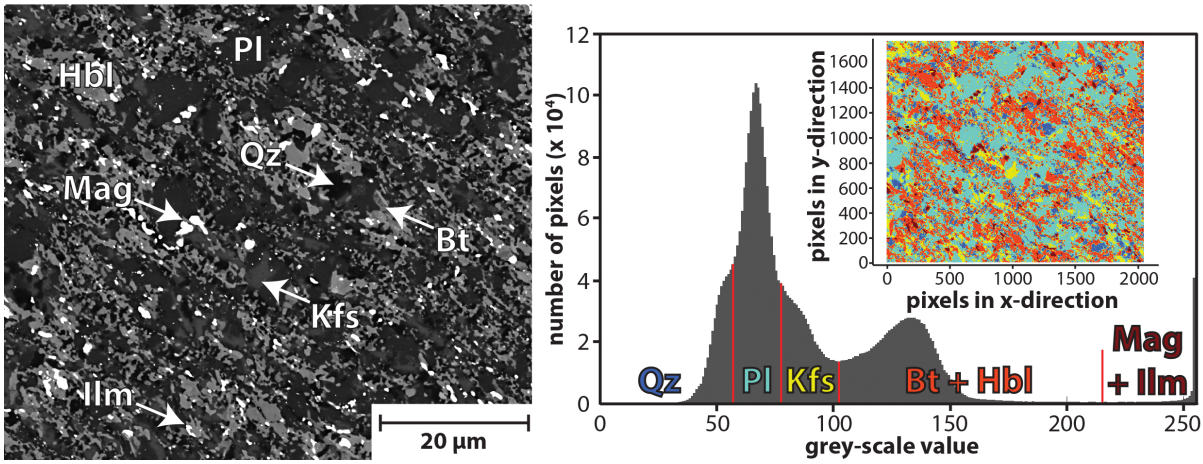

Figure S3: Calculation of the modal abundance of hydrous minerals from a BSE image. Thresholds (red lines) were set between the individual grey scale values ranges defined by each mineral. Thin section is not oriented. Sample FW13-093 (coordinates: 131.45213, -25.85455; location 3 in Fig. 1 of the main paper).

S1.3 Modal abundance of hydrous minerals

The modal abundance of hydrous minerals in thin section was quantified by running an image analysis script in Matlab R2013a (Fig. S3). Utilizing BSE images, thresholds were manually defined between the individual grey scale values ranges defined by each mineral. The modal abundance of each phase was calculated after subtracting all pixels that were not part of the stable mineral assemblage (e.g. holes and clasts in pseudotachylytes). The magnification was kept roughly constant at an image width between 60-80 µm.

S1.4 Calcite isotope analysis

Carbon ($\delta^{13}C_{Cal}$) and oxygen ($\delta^{18}O_{Cal}$) isotope analysis of fine-grained, syn-tectonically crystallized calcite has been performed using a GasBench II preparation device connected to a Delta V mass spectrometer (both ThermoFisher Scientific, Bremen) at the Geological Institute at ETH, Zurich. The analytical procedures follow Breitenbach and Bernasconi (2011). Due to the low concentrations of calcite, slight modifications to these procedures include an increase in the amount of analysed sample material (9-13 mg) and utilized orthophosphoric acid (eight droplets) as well as the use of larger vials (12 ml). The data are reported in the conventional delta notation with respect to the V-PDB (Vienna Pee Dee Belemnite) and V-SMOW (Vienna Standard Mean Ocean Water) standard. For a reliable signal the benchmark Amplitude 44 (Ampl 44) should be above 2000.

S1.5 Whole rock carbon isotope analysis

Whole rock carbon isotopy ($\delta^{13}C_{whole\ rock}$) was determined using a ThermoFisher Flash-EA 1112 coupled with a Conflo IV interface to a ThermoFisher Delta V isotope ratio mass spectrometer (IRMS). Samples were combusted in the presence of oxygen in an oxidation column at 1020 °C. Combustion gases are passed through a reduction column (650 °C), and produced nitrogen and carbon dioxide gases separated chromatographically and transferred to the IRMS via an open split for on-line isotope measurements. Isotope ratios are reported in the conventional delta notation with respect to the V-PDB (Vienna Pee Dee Belemnite) standard. The system is calibrated with NBS22 ($\delta^{13}C$ = -30.03 ‰) and IAEA CH-6 ($\delta^{13}C$ = -10.46 ‰). Reproducibility of the measurements is better than 0.2 ‰. For a reliable signal the benchmark Amplitude 44 (Ampl 44) should be above 2000.

S2 Calcite and whole rock stable isotopic signature

In an attempt to constrain the origin of the ~~hydrothermally~~ introduced carbon (Fig. 7c of the main paper), felsic and mafic samples, with and without fine-grained, syn-tectonically crystallized calcite, have been isotopically analysed (for details on the methods see Supporting Information S1), with the results for $\delta^{13}C_{Cal}$, $\delta^{18}O_{Cal}$, and $\delta^{13}C_{whole\ rock}$ summarized in Table S1. With the exception of SW13-173A, calcite isotopic signatures were obtained for all calcite-bearing samples, yielding $\delta^{13}C_{Cal}$ (V-PDB) values between -2.7 ‰ to -5.9 ‰ (mean average -4.1 ‰) and $\delta^{18}O_{Cal}$ (SMOW) values between +5.7 ‰ and +14.5 ‰ (mean average +10.1 ‰). Within the same samples, the $\delta^{13}C_{whole\ rock}$ (V-PDB) isotopic signature is always lower (on average by 2.7 ‰) than the corresponding $\delta^{13}C_{Cal}$ values. Calcite-free samples yield significantly lower $\delta^{13}C_{whole\ rock}$ values between -10.7 ‰ and -22.6 ‰ (Table S1), with this carbon presumably coming from CO_2 contained in fluid inclusions. The amplitude (Ampl 44) of each measurement functions as a benchmark for the data's reliability. This parameter should typically be above 2000 for a measurement to be considered trustworthy. Consequently, $\delta^{13}C_{Cal}$ and $\delta^{18}O_{Cal}$ of SW13-159 and NW14-408 are well constrained, whereas the results for NW13-203, SW14-025 and SW13-124 are less reliable. The low benchmark values almost certainly reflect the very low modal abundance of calcite in the studied rocks (typically <1 %). Nevertheless, the determined values for each of the five samples are reproducible in different runs and are very similar to each other, which argues for their reliability.

					GasBench II					Combustion	
	location	sample	lithology	coordinates	$d^{13}C_{cal}$(‰)		$d^{18}O_{cal}$ (‰)			$d^{13}C_{whole\ rock}$ (‰)	
	(Fig. 1)			(WGS 1984)	run	(V-PDB ± 2σ)	(V-PDB ± 2σ)	(SMOW)	Ampl 44	(V-PDB)	Ampl 44
calcite-bearing	9 (HW)	NW13-203	granite	131,74318 -26,00442	1	-4,12 ± 0,15	-21,19 ± 0,23	9,02	686	-9,36	4235
					2	-4,12 ± 0,08	-21,34 ± 0,25	8,86	936		
					3	-4,47 ± 0,10	-23,30 ± 0,13	6,84	872		
					4	-4,08 ± 0,12	-23,56 ± 0,11	6,57	852		
	9 (HW)	SW14-025	granite	131,73269 -26,01569	1	-4,11 ± 0,34	-24,37 ± 0,25	5,74	432	-6,54	7500
					2	-3,92 ± 0,05	-24,25 ± 0,23	5,86	667		
	10 (FW)	NW14-408	dolerite	131,85345 -26,11036	1	-5,83 ± 0,05	-19,90 ± 0,15	10,34	2120	-6,83	8069
					2	-5,85 ± 0,10	-19,90 ± 0,08	10,35	3463		
	12 (FW)	SW13-124	granite	131,87272 -26,20402	1	-3,72 ± 0,14	-18,33 ± 0,29	11,97	625	-6,50	6110
					2	-3,77 ± 0,12	-18,16 ± 0,04	12,14	1099		
	14 (FW)	SW13-159	felsic gneiss	131,77375 -26,30666	1	-2,76 ± 0,07	-16,01 ± 0,16	14,36	1569	-4,88	5743
					2	-2,71 ± 0,07	-15,88 ± 0,04	14,49	2305		
	2 (-)	SW13-173A	felsic gneiss	131,45334 -25,84543	1	- -	- -	-	5313	-10,68	2353
					2	- -	- -	-	5312		
calcite-free	7 (FW)	SW13-104	granite	131,63509 -25,94122	1	- -	- -	-	7153	-22,56	983
					2	- -	- -	-	7156		
	13 (FW)	SW14-194	dolerite	131,82577 -26,24931	1	- -	- -	-	5297	-22,61	838
					2	- -	- -	-	5292		
	14 (HW)	SW13-166	dolerite	131,77451 -26,30822	1	- -	- -	-	5304	-17,29	960
					2	- -	- -	-	5294		

Table S1: Calcite ($\delta^{13}C_{Cal}$, $\delta^{18}O_{Cal}$) and whole rock ($\delta^{13}C_{whole\ rock}$) stable isotope results for the central Musgrave Block. Abbreviations: hanging wall (HW), footwall (FW).

$\delta^{13}C_{Cal}$ should provide information on the fluid~~brine~~ source, since there are no other carbon-bearing phases in the studied rocks (Collerson et al., 1972; Major, 1973; Major and Conor, 1993; Scrimgeour and Close, 1999). $\delta^{18}O_{Cal}$, on the other hand, should reflect the calcite crystallization temperatures. Our results are in agreement with the range of $\delta^{18}O$ values for metamorphic waters (Taylor, 1997, his Fig. 6.4) and carbonates (Coplen et al., 2002, their Fig. 6) at temperatures of 500-600 °C, considering that the corresponding fluid phase should isotopically have been ca. 5-6 ‰ heavier than the crystallizing calcite (Chacko et al., 1991). Our $\delta^{13}C_{Cal}$ results strongly overlap with the typical range of values for a rock-buffered system within igneous and metamorphic rocks (Coplen et al., 2002, their Fig. 4). However, from Table S1 it is evident that $\delta^{13}C_{Cal}$ is never identical to $\delta^{13}C_{whole\ rock}$. Consequently, full rock-buffering has not been achieved and it should be possible to place some constraints on the potential carbon source. The range of determined $\delta^{13}C_{Cal}$ values excludes a marine origin (Coplen et al., 2002, their Fig. 4), but is in agreement with a mantle (Deines, 2002; Javoy et al., 1986) or sedimentary source (Bitter Springs Formation; Hill et al., 2000). Within the underlying Amadeus Basin sediments, the most likely source would have been either the carbonate-bearing Bitter Springs Formation or its lateral equivalent the Pinyinna Beds (Wells et al., 1970; Young et al., 2002). However, both units do not crop out in the study area and, as outlined in Sect. 8.3.1 of the main paper, the Amadeus Basin sediments were potentially only imbricated below the Kelly Hills klippe after shearing on the Woodroffe Thrust had largely ceased. ~~Hence, the CO_2-dominated brines are likely mantle-derived.~~

S3 Hydrous minerals in felsic pseudotachylytes

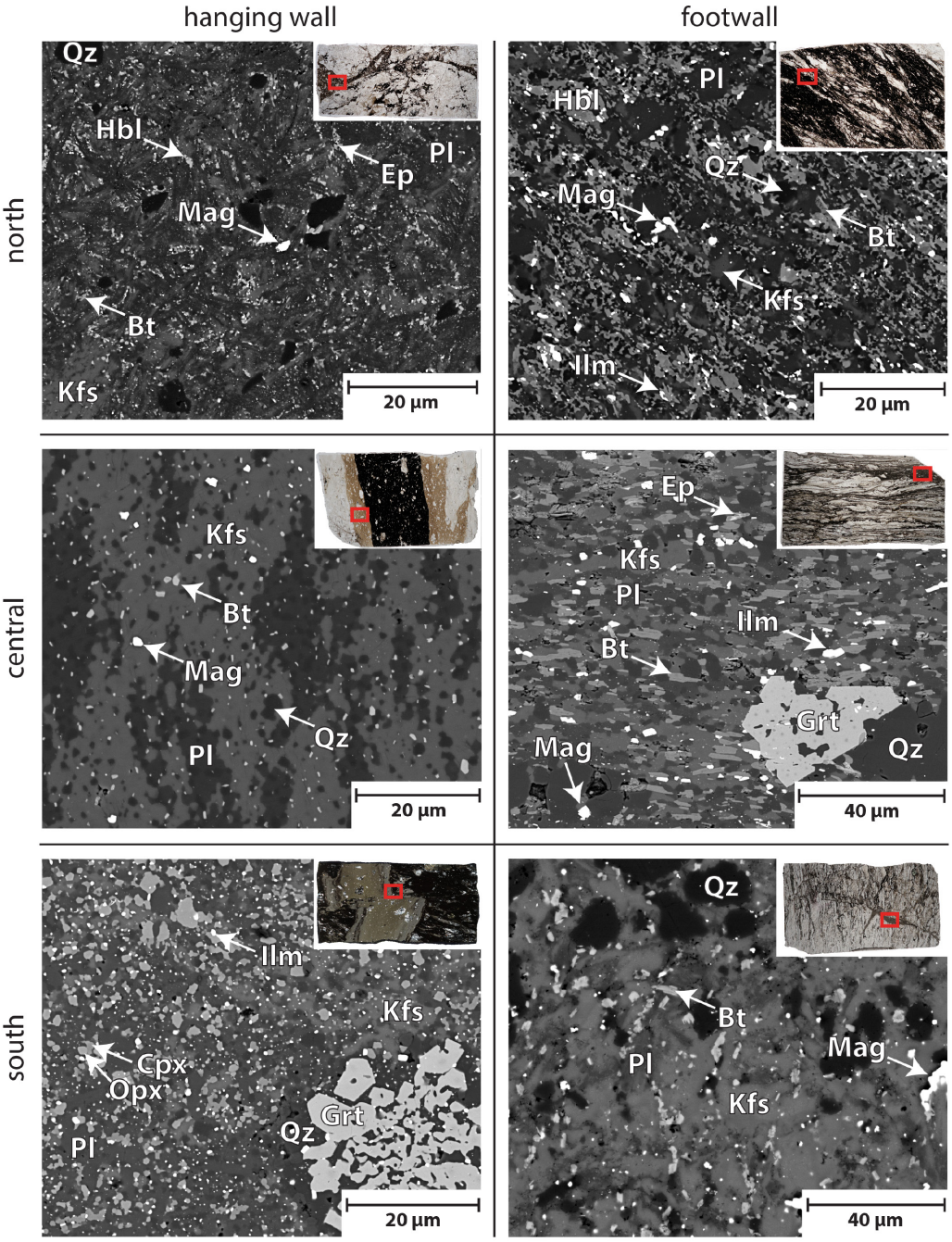

Figure S4: Representative BSE images of felsic pseudotachylytes from the hanging wall and footwall of the Woodroffe Thrust arranged into northern ~~(locations 1-5 in Fig. 1 of the main paper)~~, central ~~(locations 6-9 in Fig. 1 of the main paper)~~ and southern location groups (~~locations 11-14 in Fig. 1~~see Table 4 of the main paper). Overview thin section images are roughly 4 cm in width. (top left) Unoriented sample FW13-096 (coordinates: 131.45034, -25.85414; location 3 in Fig. 1 of the main paper). (top right) Unoriented sample FW13-093 (coordinates: 131.45213, -25.85455; location 3 in Fig. 1 of the main paper). (centre left) Unoriented sample SW14-029A (coordinates: 131.74496, -26.00093; location 9 in Fig. 1 of the main paper). (centre right) Sample SW13-321 (coordinates: 132.14333, -25.99178; location 6 in Fig. 1 of the main paper). Thin section is oriented N-S (left-right). (bottom left) Loose sample SW14-181B (coordinates: 131.92595,

-26.17664; location 11 in Fig. 1 of the main paper). (bottom right) Unoriented sample SW14-237C (coordinates: 131.83544, -26.25303; location 13 in Fig. 1 of the main paper).

S4 Plagioclase stability microstructure 3

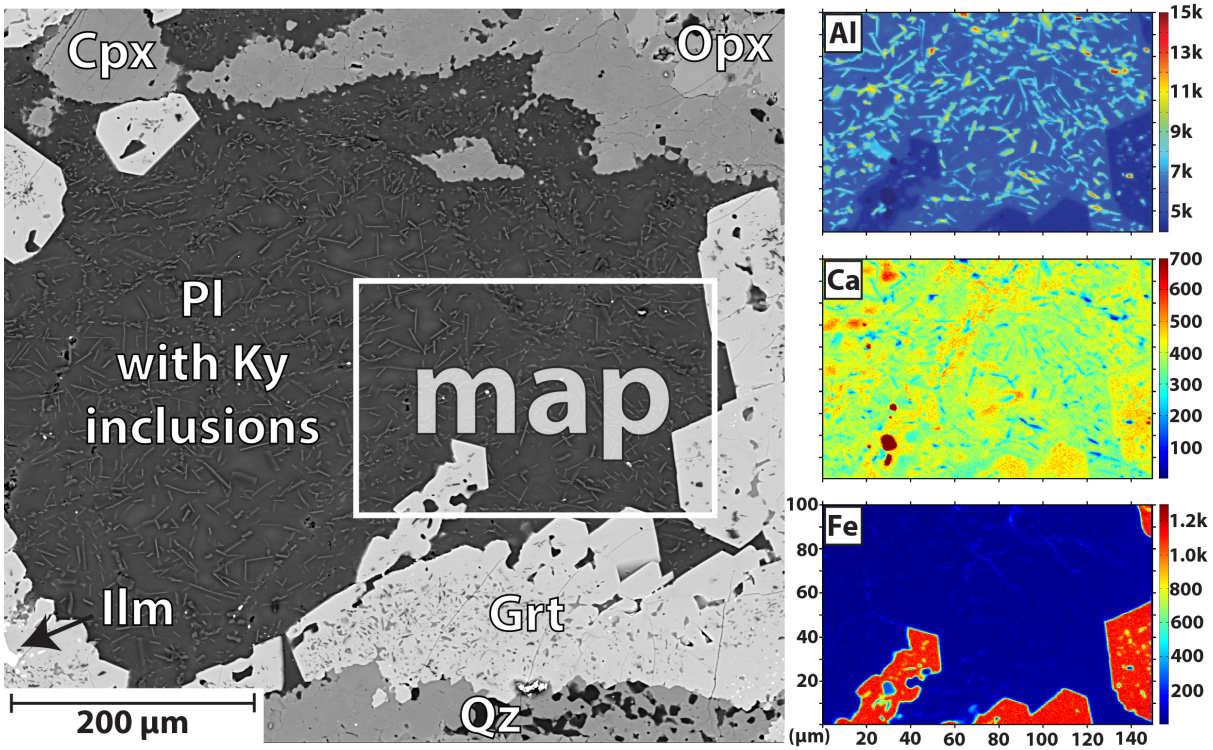

125 **Figure S5: BSE image of plagioclase with kyanite inclusions (microstructure 3). Elemental maps (Al, Ca, Fe) do not indicate the presence of epidote. The host rock is a statically overprinted dolerite dyke with a stable mineral assemblage of Pl + Cpx + Grt + Ilm + Ky + Rt + Qz. Relict orthopyroxene is locally present (top right corner). Thin section is not oriented. Sample SW13-167 (coordinates: 131.77475, -26.30845; location 14 in Fig. 1 of the main paper).**

S5 deleted